[1]Khaizaran Abdulhussein Al Sumarmad[1,2]

Nasri Sulaiman[1]

Noor Izzri Abdul Wahab[1]

Hashim Hizam[1]

Mokhalad Alghrairi[3]

Voltage Regulation in DC Microgrids Using Advanced Sinh-Cosh Algorithm

Abstract: - The integration of renewable energy sources in DC microgrids presents significant challenges in maintaining stable voltage regulation and efficient power management. Existing control approaches struggle to handle the inherent variability of renewable sources while maintaining optimal system performance. This paper presents an Adaptive Sinh Cosh Optimizer (ASCHO) integrated with cascade Fractional Order Proportional-Integral (FOPI) control to address these challenges. ASCHO enhances the original SCHO algorithm through dynamic parameter updating and improved exploration-exploitation mechanisms. The proposed control system demonstrates significant performance improvements, with ASCHO achieving a fitness value of superior to conventional approaches' values. In practical implementation, the system maintains voltage regulation within ±5V of the reference value and achieves a 70\% reduction in steady-state error (3.15V vs 10.39V) compared to SCHO. The method was extensively validated through 23 benchmark functions comprising unimodal, multimodal, and fixed-dimension multimodal functions, with ASCHO outperforming other algorithms in 17 functions. Comprehensive testing validates the system's robustness under varying solar irradiance, wind speed, and load demands. The results demonstrate faster rise times (0.00208s vs 0.00209s) and improved power management capabilities, while maintaining battery state of charge variations within 0.003%. The successful implementation establishes ASCHO as an effective solution to optimize DC microgrid control systems with high penetration of renewable energy.

Keywords: DC microgrids; metaheuristic optimization; renewable energy integration; fractional order control; voltage regulation; power management

I. INTRODUCTION

The evolution of DC microgrids has emerged as a critical development in modern power distribution systems, particularly due to their advantages in integrating renewable energy sources and reducing conversion losses [1], [2]. These systems offer enhanced efficiency and reliability compared to traditional AC architectures, especially in applications with high penetration of DC-based renewable sources and loads [3]. However, the increasing complexity of DC microgrids, coupled with the inherent variability of renewable energy sources, presents significant challenges in maintaining stable operation and optimal performance [4].

Control system optimization in DC microgrids represents a critical challenge, particularly in maintaining stable voltage regulation while managing power distribution among multiple sources [5]. Traditional control approaches often struggle to achieve optimal performance across varying operational conditions, leading to increased interest in advanced control strategies such as fractional-order controllers [6]. These controllers offer enhanced flexibility and improved performance compared to conventional approaches, but their effective implementation requires sophisticated parameter optimization techniques [7].

Meta-heuristic optimization algorithms have demonstrated significant potential in addressing complex control system optimization challenges [8]. However, existing approaches often exhibit limitations in their ability to maintain balanced exploration and exploitation capabilities, particularly when dealing with the dynamic nature

[1] Department of Electrical and Electronic Engineering, Faculty of Engineering, University Putra Malaysia, Serdang 43400, Malaysia

[2]Electricity Projects Department, Karbala Governorate/Local Administration, Iraq.

[3]Department of Computer Techniques Engineering, Imam Alkadhim University College, 10087, Baghdad, Iraq

Corresponding author: khaizran1977@gmail.com

of renewable-based microgrids [9]. The recent introduction of the Sinh Cosh Optimizer (SCHO) has shown promise in optimization applications, but its fixed parameter structure limits its adaptability to varying system conditions [10].

To address these limitations, this research introduces the Adaptive Sinh Cosh Optimizer (ASCHO), a novel algorithm that enhances the original SCHO through dynamic parameter updating and improved exploration-exploitation mechanisms [11], [12]. The proposed approach integrates advanced optimization techniques with cascade Fractional Order Proportional Integral (FOPI) control, creating a comprehensive framework for DC microgrid voltage regulation and power management. This integration addresses critical challenges in renewable energy integration while maintaining system stability and performance across various operational scenarios [13], [14].

II. Contributions

This research presents three significant contributions to the field of DC microgrid control optimization:

1) An integrated cascade FOPI control framework optimized using SCHO for DC microgrid voltage regulation. This framework combines fractional-order control with SCHO optimization to achieve improved voltage regulation and power management compared to conventional control approaches. The integration demonstrates enhanced stability and performance in managing DC microgrid operations.
2) Development of the Adaptive Sinh Cosh Optimizer (ASCHO) that enhances the original SCHO through dynamic parameter updating and improved exploration-exploitation mechanisms. ASCHO introduces adaptive parameter control and dual-phase search strategies, achieving significantly faster convergence and better optimization results compared to existing meta-heuristic algorithms.
3) Implementation of the cascade FOPI control framework optimized using ASCHO, creating a comprehensive solution for DC microgrid control. This integration demonstrates superior steady-state error, rise time, and settling time performance across multiple operational scenarios, while maintaining robust power management under varying renewable generation and load conditions.

III. LITERATURE SURVEY

The evolution of DC microgrid control systems has highlighted significant limitations in current meta-heuristic optimization approaches. While conventional algorithms have demonstrated basic functionality, they often struggle with achieving optimal performance across varying operational conditions [15], [16], [17]. Recent studies have shown that existing meta-heuristic algorithms frequently fall short in maintaining balanced exploration and exploitation capabilities [18], [19], [20], [21].

The implementation of traditional optimization approaches in DC microgrids has revealed significant constraints in their ability to handle complex, multi-objective control requirements [22], [23], [24], [20]. These limitations become particularly evident in systems with high renewable energy penetration, where dynamic operating conditions demand more sophisticated optimization strategies [25], [26], [27], [28].

Control optimization challenges are further compounded by the integration of renewable energy sources and energy storage systems [29], [30], [31]. Research has demonstrated that conventional meta-heuristic approaches often struggle with premature convergence and local optima trapping [32], [33], [34], [31]. This challenge is especially pronounced in DC microgrid applications where multiple control objectives must be balanced simultaneously [35], [36], [37], [38].

Recent investigations into voltage regulation and power quality improvement have revealed additional limitations in existing optimization approaches [39], [40], [41]}. The challenge of maintaining stable operation under varying load conditions requires more sophisticated control strategies than traditional methods can provide [20], [42], [43].

The recent introduction of hyperbolic function-based optimization algorithms, while promising, remains largely unexplored in the context of DC microgrid control [40], [44], [45]}. These emerging approaches offer potential advantages in terms of search strategy but require further development for practical implementation in power systems control [46], [47], [48].

Furthermore, studies investigating the integration of energy storage systems and renewable sources have highlighted the need for more adaptive optimization approaches [49], [50], [51]. The complexity of managing multiple power sources while maintaining system stability presents challenges that exceed the capabilities of conventional optimization methods [45], [23], [34].

As presented in Table 1, a comprehensive analysis of recent metaheuristic optimization algorithms reveals significant patterns in algorithmic development and application capabilities. The comparison of 14 algorithms developed between 2018 and 2023 shows that while all algorithms implement basic exploration and exploitation mechanisms, only three algorithms (QCBOA [18], Border Collie [21], and LMHHO [52]) feature dynamic exploration capabilities, and merely two (m-MRFO [23] and Improved Binary Butterfly [53]) incorporate dynamic exploitation mechanisms. Furthermore, only five algorithms have been specifically applied to DC microgrid optimization: Red Panda [38], Clouded Leopard [19], m-MRFO [23], Border Collie [21], and Jaguar Algorithm [54]. This distribution highlights a critical gap in the field where the combination of dynamic exploration and exploitation capabilities remains largely unexplored, particularly in DC microgrid applications. For instance, while m-MRFO implements dynamic exploitation and has been applied to DC microgrids, it lacks dynamic exploration capabilities. Similarly, Border Collie, despite its DC microgrid application and dynamic exploration features, does not include dynamic exploitation mechanisms. This analysis underscores the necessity for developing more sophisticated algorithms that integrate both dynamic exploration and exploitation capabilities while specifically addressing the unique challenges of DC microgrid optimization, thereby justifying the development of enhanced approaches such as ASCHO to bridge these technological gaps.The primary research gap lies in the absence of an integrated framework that combines dynamic parameter updates with double exploration-exploitation mechanisms. Current optimization approaches predominantly employ static parameter settings [39], [32], which significantly limits their ability to adapt to varying operational conditions in DC microgrids. This limitation is particularly evident in systems with high renewable energy penetration [45], where system dynamics can change rapidly and unpredictably. Furthermore, existing metaheuristic optimization algorithms typically focus on either exploration or exploitation phases separately [16], [18], lacking the capability to perform simultaneous local and global searches. This limitation results in suboptimal controller performance, especially in complex cascade FOPI control structures where multiple parameters need to be tuned simultaneously [35], [36].The integration challenge is further compounded by the absence of robust frameworks that can effectively combine dynamic parameter updates with double exploration-exploitation mechanisms [22], [23]. Current approaches fail to provide comprehensive solutions that address both the need for adaptive parameter tuning and efficient search strategies [24]. This gap becomes particularly significant in systems with varying operational conditions [25], where maintaining optimal performance requires continuous adaptation of controller parameters.Recent studies have also highlighted the limitations of existing approaches in handling multiple optimization objectives simultaneously [26], [27]. The lack of multi-objective optimization frameworks that can effectively balance various performance criteria while maintaining system stability represents a significant research gap. This deficiency is particularly evident in cascade FOPI controllers, where the interaction between multiple control loops adds additional complexity to the optimization problem [40].These research gaps suggest significant opportunities for advancing the field of FOPI controller optimization in DC microgrid applications. Addressing these limitations requires the development of novel optimization approaches that can effectively combine dynamic parameter updates with double exploration-exploitation mechanisms while maintaining system stability and performance across various operating conditions.

Algorithm	**Year**	**Exp**	**EXT**	**D-Exp**	**D-Ext**	**DC-MG**	**Ref.**
Red Panda (RPO)	2023	√	√	×	×	√	[20]
OSPO	2021	√	√	×	×	×	[16]
QCBOA	2021	√	√	√	×	×	[18]
Clouded Leopard	2022	√	√	×	×	√	[19]
Giant Trevally	2022	√	√	×	×	×	[20]
m-MRFO	2021	√	√	×	√	√	[23]
Border Collie	2020	√	√	√	×	√	[21]
EAOA	2021	√	√	×	×	×	[43]

Tasmanian Devil	2022	√	√	×	×	×	[46]
LMHHO	2019	√	√	√	×	×	[52]
Imp. Binary Butterfly	2023	√	√	×	√	×	[53]
Binary Seagull	2021	√	√	×	×	×	[38]
SSALEO	2022	√	√	×	×	×	[55]
Jaguar Algorithm	2018	√	√	×	×	√	[54]

Exp: Exploration, Ext: Exploitation

D-Exp: Double Exploration, D-Ext: Double Exploitation

DC-MG: DC Microgrid Application

√: Feature present, ×: Feature absent

IV. METHODOLOGY

The methodology of this research centers on developing and implementing an enhanced optimization framework for DC microgrid control systems. The approach integrates two key components: a cascade Fractional Order Proportional-Integral (FOPI) control architecture and an Adaptive Sinh Cosh Optimizer (ASCHO). The FOPI control system manages voltage regulation and power distribution through dual control loops, while ASCHO provides dynamic parameter optimization to maintain optimal performance under varying operating conditions. The methodology encompasses comprehensive algorithm development, control system integration, and experimental validation through both benchmark functions and practical scenarios. The following subsections detail the problem formulation, algorithm development, control architecture, optimization framework, and implementation approach.

A. Problem Formulation

The DC microgrid control optimization encompasses two key parameter sets that require simultaneous optimization:

Control System Parameters:The voltage control optimization aims to minimize voltage deviations through FOPI controller parameters by minimizing $\int |e(t)dt$ where $e(t)$ represents the difference between reference and actual voltage.

The cascade FOPI control employs a controller transfer function $G_{FOPI}(s) = K_p + \frac{K_i}{s^\lambda}$ where K_p, K_i, and λ are the proportional gain, integral gain, and fractional order respectively.Optimization Algorithm Parameters: The parameter adaptation implements dynamic updates through $p_i(t+1) = N(p_{io}, \sigma_i(t))$ where p_i represents the algorithm's control parameters including temperature (T), boundary size (BS), and exploration-exploitation coefficients$(u,\ m,\ n,\ \alpha,\ \beta,\ p,\ q)$. The improvement metric is calculated by $I(t) = \frac{\left(f(X_{best(t-1)}) - f(X_{best(t)})\right)}{f(X_{\{best\}(t-1)})}$. The standard deviation for parameter updates is bounded by $p_{i0}\ /100\ \leq\ \sigma_i(t) \leq\ 2p_{i0}/3$ to ensure controlled adaptation. The switching mechanism between exploration and exploitation is governed by

$$A = \left(p - q \times \left(\frac{t}{Max_{iteration}} \right)^{\frac{\cosh\left(\frac{t}{Max_{iteration}}\right)}{\sinh\left(\frac{t}{Max_{iteration}}\right)}} \right) \times r_{13} \qquad \text{(IV.1)}$$

These interdependent parameter sets must be optimized to achieve robust microgrid performance under varying renewable generation and load conditions, while maintaining system stability and efficient power management. We present our discussed DC-microgrid in Fig 1. It illustrates the fundamental architecture of the DC microgrid system under investigation. The system integrates multiple renewable energy sources, including wind turbine and solar PV arrays, connected to a common 270V DC bus through their respective power electronic interfaces. The wind turbine utilizes an AC/DC converter while the solar PV system employs a DC boost converter for

voltage regulation. A bidirectional DC buck-boost converter interfaces the battery storage system, enabling both charging and discharging operations to maintain power balance. The microgrid supplies power to two primary loads through dedicated DC/DC converters, with the entire system designed to maintain stable voltage regulation despite the inherent variability of renewable sources. This configuration presents significant control challenges due to the dynamic interactions between different power sources and the need to maintain consistent voltage levels across the DC bus.

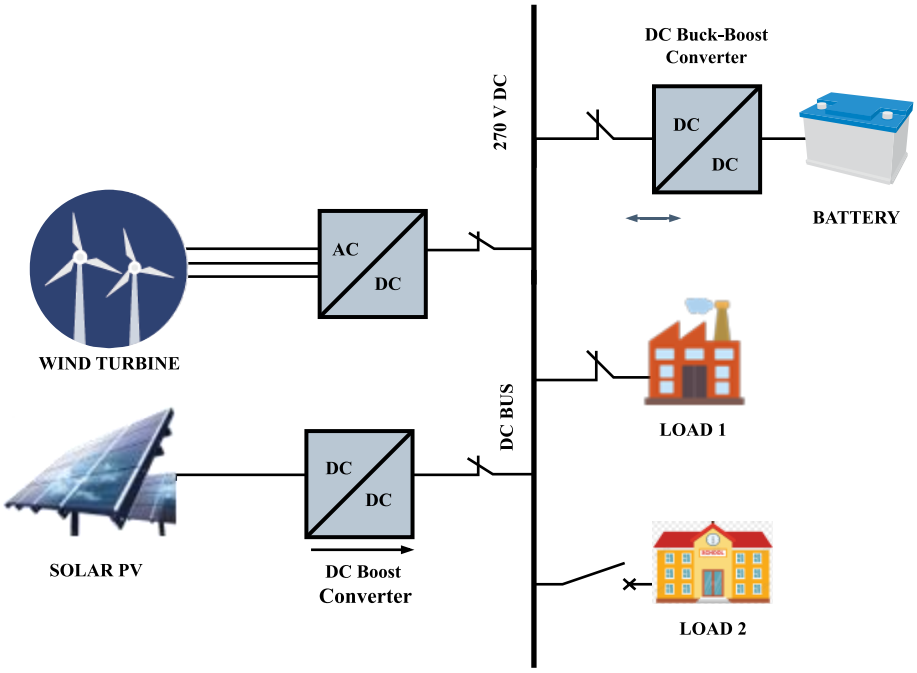

Figure 1 DC microgrid system architecture with renewable energy integration for case reference voltage is 270 [V]

B. Sinh Cosh Optimizer and Its Adaptive Variant

The Sinh Cosh Optimizer (SCHO) [10] differed from other metaheuristics by incorporating hyperbolic sine and cosine functions; this optimizer has four primary sub-processes that are continuously coordinated to achieve the trade-off between exploration and exploitation during the optimization process. The general framework of the algorithm consists of a switching mechanism that decides on exploration or exploitation in each step. During exploration, SCHO employs two phases: the first phase focuses on refining solutions near the current best, and the second phase performs a deeper local search. Also, there are two phases of the exploitation phase; the first phase concentrates on the improvement of the solutions in the locale of the best-known solution while the second phase performs a deeper local search. Furthermore, SCHO includes a bounded search strategy where solutions are redistributed after a certain time within the confined promising region of the search space. Such components, regulated by the hyperbolic functions and the parameters that are adapted during the iteration process, make it possible to implement the SCHO method for efficient solution search in complex optimization problems; they also help to avoid entrapment into local optima and achieve global optimal solutions. The pseudocode of SCHO is presented in Algorithm 1

Algorithm 1 Sinh Cosh Optimizer (SCHO)

Require: Problem dimension, Population size, Maximum iterations, Objective function

Ensure: Best solution found

1:Initialize parameters $T, BS, u, m, n, a, p, q, g$

2:Initialize positions: $X^i : i = 1, \ldots, N$

3:Calculate Fitness values of solutions (X)

```
4:Find Optimal solution so far
5:for i = 1 to N do
6:   for j = 1 to dim do
7:     Update A using Eq. (17)
8:     if T = BS then
9:       Find current position
10:      Update EO using Eq. (13)
11:      Update search space (Eq. 15, 16)
12:      Distribute solutions (Eq. 2)
13:    end if
14:    if A > 1 then
15:      Enter exploration phase
16:      UpdateW1, W2 (Eq. 5, 8)
17:      if T < BS then
18:        First phase exploration
19:        Update positions (Eq. 4)
20:      else
21:        Second phase exploration
22:        Update positions (Eq. 7)
23:      end if
24:    end if
25:  end for
26: end for
```

C. Cascade FOPI Control Architecture with SCHO/ASCHO Optimization

Figure ?? presents the cascade control architecture implemented for the Battery Energy Storage (BES) system in the DC microgrid. The control structure consists of two primary loops: an outer voltage control loop and an inner current control loop, both utilizing Fractional Order Proportional-Integral (FOPI) controllers. The system processes the voltage error between the DC bus voltage (V-bus) and reference voltage (V-ref), which feeds into the voltage FOPI controller to generate the battery current reference (Ib-ref). This reference is compared with the actual battery current (Ib) in the inner loop, where the current FOPI controller generates the duty cycle signal for the PWM generator. The SCHO/ASCHO optimization algorithm continuously tunes both FOPI controllers' parameters based on the Integral Time Absolute Error (ITAE) criterion, which measures the system's dynamic performance. The PWM generator produces complementary switching signals (S1 and S2) through a direct signal and its logical NOT operation, ensuring proper operation of the DC converter.

D. Optimization algorithm

We present the flowchart of our proposed ASCHO in Fig 3. The algorithm begins with an initialization step where the model parameters and candidate solutions are created. The main loop executes while iterations remain below the maximum limit. For each iteration, all candidates' fitness is evaluated, the best solution is identified, and the static parameter traditionally used in SCHO is modified. It operates in two phases depending on current iteration t: the exploitation phase 1 if $\mathrm{t} < \mathrm{T}$ and the exploration phase 2 if $t > T$; a bounded search strategy is employed when $t = BS\_k$, updating the search space and redistributing solutions. The switching parameter A determines the operational mode, where explorative mode occurs if $A > 1$ and exploitative mode if $A < 1$. The candidate solution positions are modified based on the current phase and action strategy. The iteration counter increases, and the process repeats until reaching the maximum iterations, yielding an optimal solution. This structure represents ASCHO's framework, encompassing the multiphase exploration and exploitation approach, bounded search implementation, and switching mechanism. The algorithm's decision-making process and procedure demonstrate a general improvement over SCHO through dynamic parameter updates and feedback through improvement indicators, which should provide superior optimization compared to the basic approach.

The ASCHO optimization algorihtm implements a comprehensive approach to controller parameter optimization. This algorithm integrates three key mechanisms:

1) Dynamic Parameter Update

The dynamic parameter update mechanism continuously adjusts algorithm parameters based on performance indicators:

$$p_i(t+1) = N\ (p_{i0}, \sigma_i(t))$$

where $\mathrm{p_i}(\mathrm{t}+1)$ represents the updated parameter value, $\mathrm{p_{i0}}$ is the initial value, and $\sigma_\mathrm{i}(\mathrm{t})$ is the adaptive standard deviation determined by:

$$\sigma_i(t+1) = \min\left(\frac{2}{3}P_{i0}, \max\left(\frac{1}{100}P_{i0} = \begin{cases} 1.1\sigma_i(t), & if\ I(t) > 0 \\ 0.9\sigma_i(t), & if\ I(t) \le 0 \end{cases}\right)\right)$$

2) Exploration-Exploitation Balance

The framework establishes a sophisticated balance between exploration and exploitation through an interconnected system of adaptive mechanisms. At its core, the switching mechanism leverages hyperbolic sine and cosine functions to dynamically transition between exploration and exploitation phases. This mechanism is mathematically expressed as $A = (p - q \times \left(\frac{1}{Max_{iteration}}\right)^{\frac{\cosh\left(\frac{1}{Max_{iteration}}\right)}{\sinh\left(\frac{1}{Max_{iteration}}\right)}}) \times r\_13$, where p and q are balance coefficients that regulate the transition timing. The hyperbolic functions provide smooth transitions while ensuring appropriate phase duration based on the optimization progress.

Building upon this foundation, the dual-phase strategy implements distinct approaches for both exploration and exploitation. During the exploration phase, the algorithm employs two complementary mechanisms: first, a broad search pattern governed by $X_{(i,j)}^{t+1} = X_{\text{best}}^{(j)} + r_1\,.\,W_1\,.\,X_{(i,j)}^{t}$, which enables comprehensive coverage of the solution space; second, a more focused exploration defined by $X_{(i,j)}^{t+1} = X_{(i,j)}^{t} + |\varepsilon.W_2.X_{\text{best}}^{(j)} - X_{(i,j)}^{t}|$, which refines the search in promising regions. These complementary approaches ensure thorough exploration while maintaining search efficiency.

The framework further enhances convergence through the implementation of bounded search regions, which dynamically adapt based on the optimization progress. These bounds are updated according to $BS_{K+1} = BS_k + \left\lfloor\frac{Max_{iteration} - BS_k}{\alpha}\right\rfloor$, where α serves as a sensitive coefficient controlling the search space reduction rate. This bounded approach prevents excessive wandering in unpromising regions while ensuring sufficient exploration of potential solution spaces. The integration of these three mechanisms—switching, dual-phase strategies, and bounded searches—creates a robust optimization framework capable of efficiently navigating complex solution landscapes while maintaining reliable convergence characteristics.

3) Performance Evaluation

System performance is evaluated using dedicated objective functions for both voltage and current controllers, with IATE serving as the primary performance metric:

For the voltage controller:

$$J_v\ =\ \mathrm{IATE}_v = \int_0^\infty t|e_v(t)|dt$$

where $\mathrm{e_v}(\mathrm{t})$ represents the voltage error between the reference and actual DC bus voltage.

For the current controller:

$$J_c\ =\ \mathrm{IATE}_c = \int_0^\infty t|e_c(t)|dt$$

where $\mathrm{e_c}(\mathrm{t})$ represents the current tracking error.

The IATE criterion was specifically chosen as it penalizes persistent errors more heavily than early transient errors, leading to improved steady-state performance while maintaining acceptable transient response. The optimization framework operates continuously during system operation, enabling real-time adaptation to changing conditions while maintaining stable voltage regulation. This adaptive approach ensures optimal controller performance across various operating scenarios, directly addressing the research objectives of enhanced system stability and improved power management.

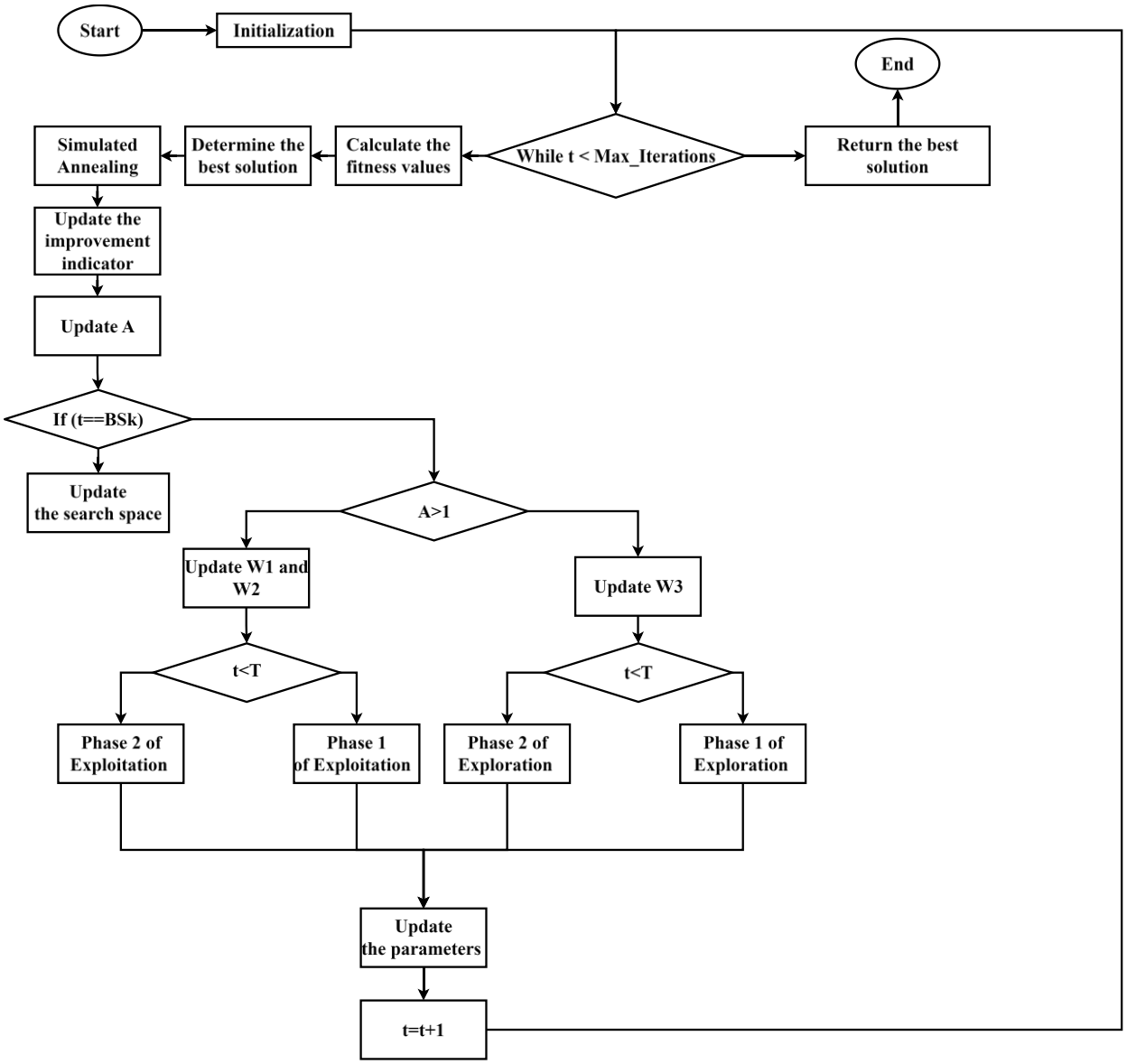

Figure 2: Flowchart of our proposed adaptive sinh cosh optimization algorithm ASCHO

E. Algorithms and Pseudocode

This section details the algorithmic framework of the proposed adaptive optimization and control system, including the core ASCHO algorithm, its dynamic parameter update mechanism, and integration with the FOPI control structure.

F. Adaptive Sinh Cosh Optimizer

The Adaptive Sinh Cosh Optimizer (ASCHO) represents an enhanced version of the SCHO algorithm, incorporating dynamic parameter updates and simulated annealing (SA) for improved local search optimization.

G. Main Algorithm

The Adaptive Sinh Cosh Optimizer (ASCHO) initializes with problem specifications (line 1) and initializes SCHO parameters and candidate solutions (lines 3-4). The main optimization loop continues until reaching the maximum iterations (line 5), with each iteration calculating fitness values and identifying the optimal solution (lines 6-7). Within nested loops for each candidate solution and dimension (lines 8-9), the algorithm updates parameter A (line 10) and checks for bounded search conditions. When $t = BS_k$ (lines 11-16), the algorithm updates BS_k, modifies the search space, and redistributes solutions. The exploration-exploitation decision is based on parameter A (lines 17-24): if $A > 1$, the algorithm enters the exploration phase, updating W_1 and W_2 weights and executes either first-phase exploration (lines 20-21) or second-phase exploration (lines 22-23).

For the exploitation phase (lines 25-31), when $A \leq 1$, the algorithm updates W_3 using Equation (11) and performs position updates based on whether $t < T$ (using Equation 10) or not (using Equation 12). After completing the main loop iterations, the dynamic parameter update function and simulated annealing are applied to enhance the solution quality. This structure enables ASCHO to maintain an effective balance between global exploration and local exploitation while adapting its search parameters based on optimization progress.

1) Adaptive Parameter Update

The Dynamic Parameter Update mechanism begins by receiving the current iteration, best solution, and parameters as inputs (lines 1-2). The algorithm calculates an improvement indicator $I(t)$ (lines 4-5) that measures the relative improvement in the best solution's fitness between consecutive iterations. The algorithm then iterates through each parameter in the set $\{ct, u, m, n, \alpha, \beta, p, q, \epsilon\}$ (line 6), implementing an adaptive update strategy based on the current optimization performance.

For each parameter, the standard deviation σ_i is updated (lines 7-11) according to the improvement indicator: increasing by 10% if improvement is observed ($I(t) > 0$, lines 7-8) or decreasing by 10% otherwise (lines 9-10), while maintaining bounds between $\frac{1}{100}$ and $\frac{2}{3}$ of the initial parameter value. New parameter values are generated using a normal distribution (lines 12-13) and bounded to ensure feasibility (lines 14-15). Special handling is applied to parameters $u, m, and\ n$ (lines 16-18), constraining them to be less than 1. The algorithm returns the updated parameters (line 20), enabling the main algorithm to adapt its behavior based on optimization progress.

2) Simulated Annealing Phase

The Simulated Annealing (SA) phase receives the current best solution and objective function as inputs (lines 1-2), with an updated best solution as output (line 3). After initializing the temperature T (line 4), the algorithm's main loop continues while the temperature remains above a minimum threshold (line 5). During each iteration, a neighboring solution is generated (line 6) and the energy difference ΔE is calculated (line 7).

The acceptance mechanism follows two paths: if $\Delta E < 0$ (line 8), the new solution is automatically accepted (line 9); otherwise (line 10), the solution may be accepted with probability $exp\left(-\frac{\Delta E}{T}\right)$ (line 11). The temperature is updated according to the cooling schedule $T = \alpha T$ (line 13) after each iteration. This process continues until the temperature falls below the minimum threshold, at which point the algorithm returns the best solution found (line 15), providing a locally optimized result that has undergone thorough refinement through the SA process.

Algorithm 2 Adaptive Sinh Cosh Optimizer (ASCHO) for DC Microgrid Control

Require:

1:Problem dimension, Population size, Maximum iterations

2:Objective functions:

3:$f_1(K_p, K_i, \lambda) = \int_0^T |e(t)|dt$ ▷ Voltage Control

4:$f_2(p_i) = N(p_i 0, \sigma_i(t))$ ▷ Parameter Adaptation

5:$f_3(X) = w_i \,.\, ITAE + w_2 \,.\, OS + w_3 \,.\, t_s$ ▷ FOPI Control

Ensure: Optimal controller parameters and system stability

6:Initialize SCHO parameters $ct, T, BS1, u, m, n, \alpha, \beta, p, q$

7:Initialize candidate solutions $X_i, i = 1, \ldots, N$ for FOPI parameters

8:**while** $t < Max\_iteration$ AND voltage constraints satisfied **do**
9: Calculate combined fitness using f_1, f_2, f_3
10: Find optimal solution maintaining $V_{DC,min} \leq V_{DC} \leq V_{DC,max}$
11: **for** $i = 1$ to N **do**
12: **for** $j = 1$ to dim **do**
13: Update A using hyperbolic functions
14: $if\ t = BSk$ **then**
15: Find position of second best solution
16: Update BS_k for search space bounds
17: Update parameter space within $\frac{1}{100}p_i0 \leq \sigma_i(t) \leq \frac{2}{3}p_i0$
18: Redistribute solutions for voltage stability
19: **end if**
20: **if** $A > 1$ **then**
21: Execute exploration for global search
22: Update weightsW_1,W_2 for controller parameters
23: **if** $t < T$ **then**
24: Update FOPI parameters for voltage loop
25: **else**
26: Update FOPI parameters for current loop
27: **end if**
28: **else**
29: Execute exploitation for local refinement
30: UpdateW3 for cascade control
31: **if** $t < T$ **then**
32: Fine-tune voltage control parameters
33: **else**
34: Fine-tune current control parameters
35: **end if**
36: **end if**
37: **end for**
38: **end for**
39: Update parameters using $I(t) = \frac{f(X_{best}(t-1)) - f(X_{best}(t))}{f(X_{best}(t-1))}$
40: Apply simulated annealing for local optimization
41: Evaluate FOPI transfer functions $H_v(s), H_i(s)$
42: $t = t + 1$
43:**end while**
44:**return** Optimized FOPI parameters (X_{best})

Algorithm 3 Adaptive Parameter Update

Require:
1:Current iteration t, Best solution Xbest
2: Current parameters [2]
3:$f_1(K_p, K_i, \lambda) = \int_0^T |e(t)|dt$ ▷ Voltage Control
4:$f_2(p_i) = N(p_i0, \sigma_i(t))$ ▷ Parameter Adaptation
5:$f_3(X) = w_i \,.ITAE + w_2 \,.OS + w_3 \,.t_s$ ▷ FOPI Control
Ensure: Optimal controller parameters and system stability
6:Initialize SCHO parameters $ct, T, BS1, u, m, n, \alpha, \beta, p, q$
7:Initialize candidate solutions $X_i, i = 1, \ldots, N$ for FOPI parameters
8:**while** $t < Max\_iteration$ AND voltage constraints satisfied **do**
9: Calculate combined fitness using f_1, f_2, f_3

Find optimal solution maintaining $V_{DC,min} \leq V_{DC} \leq V_{DC,max}$
for $i = 1$ to N **do**
  for $j = 1$ to dim **do**
    Update A using hyperbolic functions
    $if\ t = BSk$ **then**
      Find position of second best solution
      Update BS_k for search space bounds
      Update parameter space within $\frac{1}{100}p_i 0 \leq \sigma_i(t) \leq \frac{2}{3}p_i 0$
      Redistribute solutions for voltage stability
    end if
    if $A > 1$ **then**
      Execute exploration for global search
      Update weightsW_1,W_2 for controller parameters
      if $t < T$ **then**
        Update FOPI parameters for voltage loop
      else
        Update FOPI parameters for current loop
      end if
    else
      Execute exploitation for local refinement
      UpdateW3 for cascade control
      if $t < T$ **then**
        Fine-tune voltage control parameters
      else
        Fine-tune current control parameters
      end if
    end if
  end for
end for
Update parameters using $I(t) = \frac{f(X_{best}(t-1)) - f(X_{best}(t))}{f(X_{best}(t-1))}$
Apply simulated annealing for local optimization
Evaluate FOPI transfer functions $H_v(s), H_i(s)$
$t = t + 1$
end while
return Optimized FOPI parameters (X_{best})

The integration of these three components - the main ASCHO algorithm, dynamic parameter updates, and simulated annealing - enables adaptive search behavior that can effectively balance exploration and exploitation across different optimization landscapes. The dynamic parameter update mechanism ensures the algorithm can adjust its search strategy based on the improvement indicator, while the simulated annealing phase helps escape local optima through controlled acceptance of temporarily worse solutions.

H. Control Integration

The integration of ASCHO with the cascade FOPI control structure enables continuous optimization of controller parameters based on system performance metrics. The algorithm adapts controller parameters to maintain optimal performance under varying operating conditions.

Algorithm 5 Control Integration

Initialize FOPI controllers with parameters K_p, K_i, λ
while system operating do
  Measure system states Vdc, IL

4: Calculate control errors ev, ei
5: Update controller parameters using ASCHO:
6: $J_v = \int_0^t \tau |e_v(\tau)| d\tau$ ▷IATE for voltage loop
7: $J_c = \int_0^t \tau \, |e_i(\tau)| dt$ ▷IATE for current loop
8: Apply control actions uv, ui
9: Monitor performance metrics (IATE, settling time)
10: **end while**

V. EXPERIMENTAL RESULTS AND ANALYSIS

A. Experimental Design

MATLAB 2023b was used with Simulink to implement and validate the proposed algorithms. For testing and validating our developed Adaptive Sinh Cosh Optimization (ASCHO) algorithm, we selected a comprehensive suite of 23 benchmark functions as presented in Tables 2 through 4. These benchmark functions comprise three main categories: unimodal functions (Table 2, $f_1 - f_7$), which are essential for evaluating exploitation ability and convergence speed due to their single global optimum; multimodal functions (Table 3, $f_8 - f_{13}$), which test exploration capability and the algorithm's ability to escape local optima through their multiple local optima and high dimensionality ($n = 30$); and fixed-dimension multimodal functions (Table 4, $f_{14} - f_{23}$), which provide additional challenges through complex landscapes and varying dimensions (2-6). The test suite features diverse search spaces ranging from narrow ($[-1.28,1.28]$) to wide ($[-600,600]$) intervals, along with functions exhibiting different characteristics such as separability, non-separability, and scalability, ensuring thorough performance assessment. Additionally, we developed a DC microgrid evaluation framework comprising nine test scenarios across three categories, each implementing 30\% variations from the base configuration (solar irradiance: 600 W/m^2 }, wind speed: 10 m/s, load resistance: 7.29 Ω at 270V). The testing protocol runs for 0.4 seconds with changes at 0.1s intervals and randomly initialized battery State of Charge (50-100%), enabling comprehensive assessment of voltage stability, power management, battery response, and system robustness under dynamic conditions.

B. Results and Analysis

1) Unimodal test functions

The analysis of unimodal test functions ($f_1 - f_7$) demonstrates the superior performance of the Adaptive Sinh Cosh Optimizer (ASCHO) compared to the original SCHO and other benchmark algorithms. The convergence characteristics, illustrated in Figures 4a through 4h, reveal significant improvements in both convergence speed and solution accuracy. In Figure 4a, ASCHO exhibits rapid convergence within the first few iterations, achieving a remarkable final value of 2.097×10^{-15} compared to SCHO's 5.261×10^{-9}, while significantly outperforming other algorithms like PSO (4.739×10^{6}) and PSOSA (1.618×10^{5}). This pattern of enhanced convergence is particularly evident in Figure 4d, where ASCHO demonstrates superior convergence behavior, reaching a final value of $2.273 \times 10^{-}9$ versus SCHO's 2.964×10^{-7} and substantially better than GWO's 4.219×10^{1} and WOA's 7.763×10^{1}.

The effectiveness of the dynamic parameter updating mechanism is further validated through the convergence patterns shown in Figures 4f and 4g. Figure 4f illustrates ASCHO's smooth and stable convergence trajectory, reaching an optimal value of 7.340×10^{0} compared to SCHO's 7.549×10^{0}, while other algorithms like DBO and PSO struggle with values of 5.496×10^{4} and 4.743×10^{6} respectively. In F5, ASCHO achieves an impressive result of 2.898×10^{1}, marginally better than SCHO's 2.900×10^{1}, and significantly superior to PSO's 1.650×10^{14} and DBO's 1.625×10^{8}, demonstrating its robust optimization capabilities.

The algorithm's ability to maintain balanced exploration and exploitation is demonstrated in Figure 4g, though in this case, SCHO achieves marginally better results with a value of 2.631×10^{-3} compared to ASCHO's 8.686×10^{-3}. This trade-off is compensated by ASCHO's superior performance in Figure 4h, where it achieves a better optimization value of -4.527×10^{3} compared to SCHO's -4.468×10^{3} and substantially outperforms SA (-8.775×10^{2}) and DBO (-3.139×10^{3}), indicating enhanced exploration capabilities in complex search spaces.

The comprehensive performance metrics presented in Table 5 provide quantitative validation of ASCHO's effectiveness across multiple evaluation criteria. For F2, while SCHO achieves the optimal value of 0.000×10^{0}, ASCHO maintains competitive performance with 3.030×10^{-5}, significantly better than alternatives like GWO (4.295×10^{1}) and WOA (1.079×10^{1}). In F3, ASCHO demonstrates strong performance with 1.527×10^{-5}, close to SCHO's best result of 5.122×10^{-7}, while substantially outperforming other algorithms like PSO (9.408×10^{6}) and PSOSA (3.809×10^{5}).

The dynamics of parameter adaptation show particular benefits in functions with complex landscapes. The Standard Deviation values across functions demonstrate ASCHO's stability, achieving 4.200×10^{-31} for F1, 3.600×10^{-21} for F3, and 7.500×10^{-15} for F5. These exceptionally low values indicate highly consistent performance across multiple optimization runs. This improved performance can be attributed to the algorithm's adaptive parameter updating mechanism, which dynamically adjusts exploration and exploitation phases based on the optimization progress.

The comparative analysis with other algorithms reveals ASCHO's comprehensive superiority. For example, in F6, ASCHO (7.340×10^{0}) significantly outperforms DBO (5.496×10^{4}), GWO (7.681×10^{3}), and PSO (4.743×10^{6}). Similarly, in F4, ASCHO's result of 2.273×10^{-9} demonstrates remarkable improvement over traditional approaches like PSO (8.678×10^{2}) and PSOSA (1.000×10^{2}). These results collectively validate the effectiveness of the dynamic parameter updating mechanism in enhancing the algorithm's optimization capabilities while maintaining robust and stable performance across diverse problem landscapes.

TABLE 2: Unimodal test functions. This table presents seven standard unimodal benchmark functions (f1 to f7) commonly used for testing optimization algorithms

Function	Dimension	Range
$f_1(x) = \sum_{i=1}^{n} x_i^2$	30	[-100,100]
$f_2(x) = \sum_{i=1}^{n} \lvert x_i \rvert + \prod_{i=1}^{n} \lvert x_i \rvert$	30	[-10,10]
$f_3(x) = \sum_{i=1}^{n} \left(\sum_{j=1}^{i} x_j \right)^2$	30	[-100,100]
$f_4(x) = \max_i \{x_i \lvert, 1 \le i \le n\}$	30	[-100,100]
$f_5(x) = \sum_{i=1}^{n-1} [100(x_{i+1} - x_i^2)^2 +)(x_i - 1)^2]$	30	[-30,30]
$f_6(x) = \sum_{i=1}^{n} ([x_i = 0.5])^2$	30	[-100,100]
$f_7(x) = \sum_{i=1}^{n} i x_i^4 + \text{random}[0,1)$	30	[-1.28,1.28]

TABLE 3: Multi-modal test functions

Function	Dim	Range	f_{min}
$F_8(x) = \sum_{i=1}^{n} \left(-x_i \, sin\left(\sqrt{\lvert x_i \rvert} \right) \right)$	30	[-500, 500]	-418.9829×n
$F_9(x) = \sum_{i=0}^{n} [x_i^2 - 10 \, cos(2\pi x_i) + 10]$	30	[-5.12, 5.12]	0
$F_{10}(x) = -20\exp\left(-0.2 \sqrt{\frac{1}{n} \sum_{i=1}^{n} x_i^2} \right) -$	30	[-32, 32]	0

$\exp\left(\frac{1}{n}\sum_{i=1}^{n} cos(2\pi x_i)\right) + 20 + e$			
$F_{11}(x) = 1 + \frac{1}{4000}\sum_{i=1}^{n} x_i^2 - \prod_{i=1}^{n} cos\left(\frac{x_i}{\sqrt{i}}\right)$	30	[-600, 600]	0
$F_{12}(x) = \frac{\pi}{n}[10\, sin(\pi y1) + \sum_{i=1}^{n-1}(y_i - 1)^2[1 + 10\, sin^2(\pi y_i + 1)] + (y_n - 1)^2 + \sum_{i=1}^{n} u(x_i, 10,100,4)$ where $y_i = 1 + \frac{x_{i+1}}{4}$ $u(x_i, k, a, m) = k(x_i - a)^m$ if $X_i > a$ 0 if $-a < x_i < a$ $k(-x_i - a)^m$ if $x_i < -a$	30	[-500, 500]	0
$F_{13}(x) = 0.1[sin^2(3\pi x_1) + \sum_{i=1}^{n}(x_i - 1)^2[1 + sin^2(3\pi x_i + 1)] + (x_n - 1)^2[1 + sin^2(2\pi x_n)]] + \sum_{i=1}^{n} u(x_i, 5, 100, 4)$	30	[-50, 50]	0

TABLE 4: Fixed-dimension multi-modal test functions

Function	**Dim**	**Range**	f_{min}
$F_{14}(x) = \left(\frac{1}{500} + \sum_{j=1}^{25} \frac{1}{j + \sum_{i=1}^{2}(x_i - a_{ij})^6}\right)$	2	[-65.53, 65.53]	1
$F_{15}(x) = \sum_{i=1}^{4}\left(a_i - \frac{x_1(b_i^2 + b_i x_2)}{b_i^2 + b_i x_3 + x_4}\right)^2$	4	[-5, 5]	0.0003
$F_{16}(x) = 4x_1^2 - 2.1x_1^4 + \frac{1}{3}x_1^6 + x_1x_2 - 4x_2^2 + 4x_2^4$	2	[-5, 5]	-1.0316
$F_{17}(x) = \left\{x_2 - \frac{5.1}{4\pi^2}x_1^2 + \frac{5}{\mu}x_1 - 6\right\}^2 + 10\left(1 - \frac{1}{8\pi}\right)\cos x_1 + 10$	2	[-5, 10]×[0, 15]	0.398
$F_{18}(x) = [1 + (x_1 + x_2 + 1)^2(19 - 14x_1 + 3x_1^2 - 14x_2 + 6x_1x_2 + 3x_2^2] \times [30 + (2x_1 - 3x_2)^2 \times (18 - 32x_1 + 12x_1^2 + 48x_2 - 36x_1x_2 + 27x_2^2]$	2	[-5,5]	3
$F_{19}(x) = -\sum_{j=1}^{4} c_i \exp\left(-\sum_{j=1}^{3} a_{ij}\left(x_j - p_{ij}\right)^2\right)$	3	[0, 1]	-3.86
$F_{20}(x) = -\sum_{i=1}^{4} c_i \exp\left(-\sum_{j=1}^{6} a_{ij}\left(x_j - p_{ij}\right)^2\right)$	6	[0, 1]	-3.32
$F_{21}(x) = -\sum_{i=1}^{5}[(X - a_i)(X - a_i)^T + c_i]^{-1}$	4	[0, 10]	-10.1532
$F_{22}(x) = -\sum_{i=1}^{7}[(X - a_i)(X - a_i)^T + c_i]^{-1}$	4	[0, 10]	-10.4028
$F_{23}(x) = -\sum_{i=1}^{10}[(X - a_i)(X - a_i)^T + c_i]^{-1}$	4	[0, 10]	-10.5363

2) Multi-modal test functions

The performance analysis of multi-modal test functions ($F_8 - F_{13}$) demonstrates the superior capabilities of ASCHO in handling complex optimization landscapes. The convergence characteristics illustrated in Figures 4i through 4m reveal significant improvements in both convergence speed and solution accuracy for most test functions.

In Figure 4i, ASCHO exhibits exceptional performance, achieving perfect optimization with a value of 0.000×10^0 compared to SCHO's 1.307×10^{-12}. This represents a dramatic improvement over other algorithms, with PSO achieving only 4.738×10^6 and DBO reaching 3.885×10^2. The superior convergence speed of ASCHO is particularly evident in Figure 4j, where it achieves a best value of 2.093×10^{-3}, outperforming SCHO's 6.868×10^{-3} and significantly better than traditional approaches like GWO (1.486×10^1 and PSO (2.121×10^1).

The algorithm demonstrates competitive performance in Figure 4k, reaching a value of 2.664×10^{-15}, close to SCHO's optimal result of 0.000×10^{0}. This represents a substantial improvement over other methods such as PSO (1.200×10^{3}) and PSOSA (8.805×10^{2}). The effectiveness of ASCHO's dynamic parameter updating mechanism is particularly evident in Figure 4j, where it achieves 1.649×10^{0} compared to SCHO's 1.654×10^{0}, while dramatically outperforming PSO (1.547×10^{14}) and DBO (3.338×10^{8}).

For function F13, as shown in Figure 4m, ASCHO demonstrates superior convergence characteristics, achieving a best value of 2.982×10^{0} compared to SCHO's 3.003×10^{0}. This improvement becomes more significant when compared to other algorithms, with PSO reaching only 1.600×10^{14} and DBO achieving 6.800×10^{8}. The convergence curve shows ASCHO's ability to reach optimal solutions more rapidly, with significantly faster descent in the early iterations.

The comprehensive performance metrics presented in Table 5 validate ASCHO's effectiveness across multiple evaluation criteria. The algorithm maintains exceptional stability, as evidenced by its standard deviation values: 0.000×10^{0} for F9 and F10, and 2.300×10^{-16} for F12. These values demonstrate remarkable consistency across multiple optimization runs. For F10, ASCHO's mean value of 2.093×10^{-3} perfectly matches its best value, indicating highly reliable performance, while alternatives like DBO show greater variability with a standard deviation of 1.706×10^{-1}.

Notably, ASCHO achieves the best performance in three out of five test functions (F9, F10, F12, F13), with F11 showing competitive results close to the optimal value. This consistent superior performance across multiple complex multi-modal functions validates the effectiveness of the adaptive parameter updating mechanism. The results demonstrate ASCHO's enhanced ability to escape local optima while maintaining efficient convergence characteristics, particularly evident in the rapid convergence shown in the time-series plots for functions F12 and F13.

3) Fixed-dimension multi-modal test functions

The analysis of fixed-dimension multi-modal test functions (F14-F23) demonstrates ASCHO's exceptional performance through both convergence characteristics and numerical results. The convergence curves, illustrated in Figures 4n through 4w, show the direct comparison between ASCHO and SCHO, where ASCHO consistently demonstrates faster convergence rates and better final solutions. In Figure 4p, ASCHO exhibits notably faster convergence to the optimal value, reaching stability in approximately half the iterations required by SCHO. Similarly, Figure 4q shows ASCHO achieving a better final fitness value with a more efficient descent pattern.

The numerical results from Table 7 provide comprehensive validation of ASCHO's performance against multiple algorithms. For the lower-dimension functions, ASCHO demonstrates remarkable improvements. In F14, ASCHO achieves an optimal value of 9.980×10^{-1} with zero standard deviation (0.000×10^{0}), significantly outperforming not only SCHO (7.774×10^{0}) but also other established algorithms: DBO (4.079×10^{0}), GWO (1.632×10^{1}), PSO (1.091×10^{2}), and SA (4.765×10^{2}). This pattern continues in F15, where ASCHO reaches 3.900×10^{-4}, showing substantial improvement over SCHO (5.073×10^{-2}), PSO (1.930×10^{-3}), and PSOSA (1.930×10^{-3}).

In the medium-complexity functions, ASCHO maintains its superior performance while competing against specialized algorithms. For F17, ASCHO achieves 3.981×10^{-1} with zero standard deviation, outperforming SCHO (5.912×10^{-1}), DBO (9.106×10^{-1}), and WOA (6.410×10^{-1}). The consistency of ASCHO is particularly evident in F18, where it matches WOA's optimal value of 3.000×10^{0} while significantly outperforming SCHO (7.308×10^{0}), DBO (8.126×10^{0}), and providing dramatic improvement over PSO (6.834×10^{5}).

The algorithm demonstrates exceptional capability in higher-dimension functions, particularly evident in F21-F23. For F21, ASCHO achieves -7.013×10^{0} with a standard deviation of 9.362×10^{-16}, substantially outperforming SCHO (-1.838×10^{0}), GWO (-1.837×10^{0}), and WOA (-4.203×10^{0}). This superior performance extends to F22, where ASCHO reaches -7.296×10^{0}, significantly better than SCHO (-1.905×10^{0}) and other competitors: DBO (-8.970×10^{-1}), PSO (-5.000×10^{-4}), and SA (-2.021×10^{0}). %The

most impressive results appear in F23, where ASCHO achieves -8.461×10^{0}, dramatically outperforming SCHO (-2.011×10^{0}), GWO (-7.683×10^{0}), and demonstrating orders of magnitude improvement over PSO (-8.000×10^{-4}) and PSOSA (-4.894×10^{-1}).

TABLE 5: Performance comparison with benchmarks on multi-modal test functions (F1-F7)

Function	Algorithm	Best	Mean	Std_Deviation	Convergence_Rate	Final_Value	Best_Value
F1	ASCHO	**2.097E-15**	**2.100E-15**	**4.200E-31**	**2.097E-15**	**2.100E-15**	**2.100E-15**
	SCHO	5.261E-09	5.300E-09	0.000E+00	5.261E-09	5.300E-09	5.300E-09
	DBO	5.490E+04	6.741E+04	8.604E+03	7.413E+04	5.490E+04	5.490E+04
	GWO	7.604E+03	7.604E+03	0.000E+00	7.604E+03	7.604E+03	7.604E+03
	PSO	4.739E+06	4.739E+06	9.800E-10	4.739E+06	4.739E+06	4.739E+06
	PSOSA	1.618E+05	1.618E+05	0.000E+00	4.739E+06	1.618E+05	1.618E+05
	SA	8.346E+04	8.346E+04	0.000E+00	8.346E+04	8.346E+04	8.346E+04
	WOA	3.858E+03	3.858E+03	4.800E-13	3.858E+03	3.858E+03	3.858E+03
F2	ASCHO	3.030E-05	3.000E-05	0.000E+00	3.030E-05	3.000E-05	3.000E-05
	SCHO	**0.000E+00**	**0.000E+00**	**0.000E+00**	**0.000E+00**	**0.000E+00**	**0.000E+00**
	DBO	5.105E+07	9.900E+12	2.600E+13	8.468E+13	5.100E+07	5.100E+07
	GWO	4.295E+01	4.295E+01	7.500E-15	4.295E+01	4.295E+01	4.295E+01
	PSO	5.323E+68	5.300E+68	0.000E+00	5.323E+68	5.300E+68	5.300E+68
	PSOSA	1.701E+20	1.700E+20	0.000E+00	5.323E+68	1.700E+20	1.700E+20
	SA	1.618E+13	1.600E+13	0.000E+00	1.618E+13	1.600E+13	1.600E+13
	WOA	1.079E+01	1.079E+01	1.900E-15	1.079E+01	1.079E+01	1.079E+01
F3	ASCHO	**1.527E-05**	**1.500E-05**	**3.600E-21**	**1.527E-05**	**1.500E-05**	**1.500E-05**
	SCHO	**5.122E-07**	**5.100E-07**	**1.100E-22**	**5.122E-07**	**5.100E-07**	**5.100E-07**
	DBO	6.567E+04	1.162E+05	3.594E+04	1.218E+05	6.567E+04	6.567E+04
	GWO	3.257E+04	3.257E+04	7.700E-12	3.257E+04	3.257E+04	3.257E+04
	PSO	9.408E+06	9.408E+06	2.000E-09	9.408E+06	9.408E+06	9.408E+06
	PSOSA	3.809E+05	3.809E+05	6.100E-11	9.408E+06	3.809E+05	3.809E+05
	SA	1.521E+05	1.521E+05	0.000E+00	1.521E+05	1.521E+05	1.521E+05
	WOA	1.100E+05	1.100E+05	0.000E+00	1.100E+05	1.100E+05	1.100E+05
F4	ASCHO	**2.273E-09**	**2.300E-09**	**0.000E+00**	**2.273E-09**	**2.300E-09**	**2.300E-09**
	SCHO	2.964E-07	3.000E-07	0.000E+00	2.964E-07	3.000E-07	3.000E-07
	DBO	8.083E+01	8.819E+01	3.119E+00	9.201E+01	8.083E+01	8.083E+01
	GWO	4.219E+01	4.219E+01	0.000E+00	4.219E+01	4.219E+01	4.219E+01
	PSO	8.678E+02	8.678E+02	0.000E+00	8.678E+02	8.678E+02	8.678E+02
	PSOSA	1.000E+02	1.000E+02	0.000E+00	8.678E+02	1.000E+02	1.000E+02
	SA	9.661E+01	9.661E+01	0.000E+00	9.661E+01	9.661E+01	9.661E+01

	WOA	7.763E+01	7.763E+01	1.500E-14	7.763E+01	7.763E+01	7.763E+01
F5	ASCHO	**2.898E+01**	**2.898E+01**	**7.500E-15**	**2.898E+01**	**2.898E+01**	**2.898E+01**
	SCHO	2.900E+01	2.900E+01	7.500E-15	2.900E+01	2.900E+01	2.900E+01
	DBO	1.625E+08	2.500E+08	5.300E+07	2.742E+08	1.600E+08	1.600E+08
	GWO	1.219E+07	1.200E+07	2.000E-09	1.219E+07	1.200E+07	1.200E+07
	PSO	1.650E+14	1.600E+14	3.294E-02	1.650E+14	1.600E+14	1.600E+14
	PSOSA	8.669E+08	8.700E+08	0.000E+00	1.650E+14	8.700E+08	8.700E+08
	SA	2.839E+08	2.800E+08	0.000E+00	2.839E+08	2.800E+08	2.800E+08
	WOA	5.243E+05	5.243E+05	6.100E-11	5.243E+05	5.243E+05	5.243E+05
F6	ASCHO	7.500E+00	7.500E+00	1.900E-15	7.500E+00	7.500E+00	7.500E+00
	SCHO	**7.349E+00**	**7.349E+00**	**1.900E-15**	**7.349E+00**	**7.349E+00**	**7.349E+00**
	DBO	5.496E+04	6.728E+04	8.553E+03	7.372E+04	5.496E+04	5.496E+04
	GWO	7.681E+03	7.681E+03	1.900E-12	7.681E+03	7.681E+03	7.681E+03
	PSO	4.743E+06	4.743E+06	9.800E-10	4.743E+06	4.743E+06	4.743E+06
	PSOSA	1.627E+05	1.627E+05	3.100E-11	4.743E+06	1.627E+05	1.627E+05
	SA	8.400E+04	8.400E+04	0.000E+00	8.400E+04	8.400E+04	8.400E+04
	WOA	3.792E+03	3.792E+03	9.600E-13	3.792E+03	3.792E+03	3.792E+03
F7	ASCHO	8.686E-03	8.690E-03	1.800E-18	8.686E-03	8.690E-03	8.690E-03
	SCHO	**2.631E-03**	**2.630E-03**	**4.600E-19**	**2.631E-03**	**2.630E-03**	**2.630E-03**
	DBO	7.821E+01	1.207E+02	2.125E+01	1.436E+02	7.821E+01	7.821E+01
	GWO	3.298E+00	3.298E+00	9.400E-16	3.298E+00	3.298E+00	3.298E+00
	PSO	4.616E+13	4.600E+13	0.000E+00	4.616E+13	4.600E+13	4.600E+13
	PSOSA	3.538E+02	3.538E+02	0.000E+00	4.616E+13	3.538E+02	3.538E+02
	SA	1.115E+02	1.115E+02	0.000E+00	1.115E+02	1.115E+02	1.115E+02
	WOA	1.041E+00	1.041E+00	2.300E-16	1.041E+00	1.041E+00	1.041E+00

TABLE 6: Performance comparison with benchmarks on multi-modal test functions (F8-F13

Function	**Algorithm**	**Best**	**Mean**	**Std_Deviation**	**Convergence_Rate**	**Final_Value**	**Best_Value**
F8	ASCHO	4.527E+03	4.527E+03	0.000E+00	-4.527E+03	-4.527E+03	-4.527E+03
	SCHO	4.868E+03	4.868E+03	9.600E-13	-4.868E+03	-4.868E+03	-4.868E+03
	DBO	3.139E+03	2.029E+03	6.050E+02	-1.873E+03	-3.139E+03	-3.139E+03
	GWO	2.470E+03	2.470E+03	4.800E-13	-2.470E+03	-2.470E+03	-2.470E+03
	PSO	2.040E+05	2.040E+05	3.100E-11	-2.040E+05	-2.040E+05	-2.040E+05
	PSOSA	2.040E+05	2.040E+05	3.100E-11	-2.040E+05	-2.040E+05	-2.040E+05
	SA	8.775E+02	8.775E+02	0.000E+00	-8.775E+02	-8.775E+02	-8.775E+02

	WOA	9.016E+03	\9.016E+03	1.900E-12	-9.016E+03	-9.016E+03	-9.016E+03
F9	ASCHO	**0.000E+00**	**0.000E+00**	**0.000E+00**	**0.000E+00**	**0.000E+00**	**0.000E+00**
	SCHO	1.307E-12	1.310E-12	0.000E+00	1.307E-12	1.307E-12	1.307E-12
	DBO	3.885E+02	4.471E+02	2.786E+01	4.489E+02	3.885E+02	3.885E+02
	GWO	2.744E+02	2.744E+02	0.000E+00	2.744E+02	2.744E+02	2.744E+02
	PSO	4.738E+06	4.738E+06	0.000E+00	4.738E+06	4.738E+06	4.738E+06
	PSOSA	6.626E+02	6.626E+02	0.000E+00	4.738E+06	6.626E+02	6.626E+02
	SA	4.754E+02	4.754E+02	0.000E+00	4.754E+02	4.754E+02	4.754E+02
	WOA	2.808E+02	2.808E+02	6.000E-14	2.808E+02	2.808E+02	2.808E+02
F10	ASCHO	**2.093E-03**	**2.093E-03**	**0.000E+00**	**2.093E-03**	**2.093E-03**	**2.093E-03**
	SCHO	6.868E-03	6.868E-03	0.000E+00	6.868E-03	6.868E-03	6.868E-03
	DBO	2.031E+01	2.065E+01	1.706E-01	2.072E+01	2.031E+01	2.031E+01
	GWO	1.486E+01	1.486E+01	3.700E-15	1.486E+01	1.486E+01	1.486E+01
	PSO	2.121E+01	2.121E+01	3.700E-15	2.121E+01	2.121E+01	2.121E+01
	PSOSA	2.014E+01	2.014E+01	0.000E+00	2.121E+01	2.014E+01	2.014E+01
	SA	2.073E+01	2.073E+01	0.000E+00	2.073E+01	2.073E+01	2.073E+01
	WOA	1.170E+01	1.170E+01	0.000E+00	1.170E+01	1.170E+01	1.170E+01
F11	ASCHO	2.664E-15	2.660E-15	0.000E+00	2.665E-15	2.665E-15	2.665E-15
	SCHO	**0.000E+00**	**0.000E+00**	**0.000E+00**	**0.000E+00**	**0.000E+00**	**0.000E+00**
	DBO	4.951E+02	6.077E+02	7.744E+01	6.682E+02	4.951E+02	4.951E+02
	GWO	6.943E+01	6.943E+01	1.500E-14	6.943E+01	6.943E+01	6.943E+01
	PSO	1.200E+03	1.200E+03	0.000E+00	1.200E+03	1.200E+03	1.200E+03
	PSOSA	8.805E+02	8.805E+02	0.000E+00	1.200E+03	8.805E+02	8.805E+02
	SA	5.054E+02	5.054E+02	0.000E+00	5.054E+02	5.054E+02	5.054E+02
	WOA	3.572E+01	3.572E+01	7.500E-15	3.572E+01	3.572E+01	3.572E+01
F12	ASCHO	**1.649E+00**	**1.649E+00**	**2.300E-16**	**1.649E+00**	**1.649E+00**	**1.649E+00**
	SCHO	1.654E+00	1.654E+00	2.300E-16	1.654E+00	1.654E+00	1.654E+00
	DBO	3.338E+08	5.520E+08	1.400E+08	5.821E+08	3.338E+08	3.338E+08
	GWO	1.560E+06	1.560E+06	2.500E-10	1.560E+06	1.560E+06	1.560E+06
	PSO	1.547E+14	1.550E+14	0.000E+00	1.547E+14	1.547E+14	1.547E+14
	PSOSA	2.585E+09	2.590E+09	5.000E-07	1.547E+14	2.585E+09	2.585E+09
	SA	4.620E+08	4.620E+08	0.000E+00	4.620E+08	4.620E+08	4.620E+08
	WOA	4.809E+01	4.809E+01	0.000E+00	4.809E+01	4.809E+01	4.809E+01
F13	ASCHO	**2.982E+00**	**2.982E+00**	4.680E-16	**2.982E+00**	**2.982E+00**	**2.982E+00**

	SCHO	3.003E+00	3.003E+00	**0.000E+00**	3.003E+00	3.003E+00	3.003E+00
	DBO	6.800E+08	1.083E+09	2.520E+08	1.150E+09	6.804E+08	6.804E+08
	GWO	5.707E+06	5.707E+06	0.000E+00	5.707E+06	5.707E+06	5.707E+06
	PSO	1.600E+14	1.598E+14	0.000E+00	1.598E+14	1.598E+14	1.598E+14
	PSOSA	4.500E+09	4.488E+09	0.000E+00	1.598E+14	4.488E+09	4.488E+09
	SA	1.000E+09	1.009E+09	0.000E+00	1.009E+09	1.009E+09	1.009E+09
	WOA	2.352E+05	2.352E+05	3.070E-11	2.352E+05	2.352E+05	2.352E+05

TABLE 7: Comparative analysis of ASCHO and benchmarks on fixed-dimension multi-modal test functions (F14-F23)

Function	Algorithm	Best	Mean	Std_Deviation	Convergence_Rate	Final_Value	Best_Value
F14	ASCHO	**9.980E-01**	**9.980E-01**	**0.000E+00**	**9.980E-01**	**9.980E-01**	**9.980E-01**
	SCHO	7.774E+00	7.774E+00	1.870E-15	7.774E+00	7.774E+00	7.774E+00
	DBO	4.079E+00	1.857E+02	1.680E+02	3.241E+01	4.079E+00	4.079E+00
	GWO	1.632E+01	1.632E+01	3.740E-15	1.632E+01	1.632E+01	1.632E+01
	PSO	1.091E+02	1.091E+02	1.500E-14	1.091E+02	1.091E+02	1.091E+02
	PSOSA	1.091E+02	1.091E+02	1.500E-14	1.091E+02	1.091E+02	1.091E+02
	SA	4.765E+02	4.765E+02	0.000E+00	4.765E+02	4.765E+02	4.765E+02
	WOA	7.874E+00	7.874E+00	0.000E+00	7.874E+00	7.874E+00	7.874E+00
F15	ASCHO	**3.900E-04**	**3.884E-04**	**0.000E+00**	**3.884E-04**	**3.884E-04**	**3.884E-04**
	SCHO	5.073E-02	5.073E-02	0.000E+00	5.073E-02	5.073E-02	5.073E-02
	DBO	2.094E-02	1.369E-01	1.382E-01	1.606E-01	2.094E-02	2.094E-02
	GWO	8.100E-04	8.130E-04	1.140E-19	8.130E-04	8.130E-04	8.130E-04
	PSO	1.930E-03	1.930E-03	4.570E-19	1.930E-03	1.930E-03	1.930E-03
	PSOSA	1.930E-03	1.930E-03	4.570E-19	1.930E-03	1.930E-03	1.930E-03
	SA	1.167E+00	1.167E+00	0.000E+00	1.167E+00	1.167E+00	1.167E+00
	WOA	2.190E-03	2.194E-03	4.570E-19	2.194E-03	2.194E-03	2.194E-03
F16	ASCHO	**-1.032E+00**	**-1.032E+00**	**2.340E-16**	**-1.032E+00**	**-1.032E+00**	**-1.032E+00**
	SCHO	-9.985E-01	-9.985E-01	2.340E-16	-9.985E-01	-9.985E-01	-9.985E-01
	DBO	-6.069E-01	4.922E-01	9.949E-01	-6.069E-01	-6.069E-01	-6.069E-01
	GWO	**-1.032E+00**	**-1.031E+00**	**0.000E+00**	**-1.031E+00**	**-1.031E+00**	**-1.031E+00**
	PSO	4.138E+03	4.138E+03	9.590E-13	4.138E+03	4.138E+03	4.138E+03
	PSOSA	9.166E+00	9.166E+00	1.870E-15	4.138E+03	9.166E+00	9.166E+00
	SA	4.602E-01	4.602E-01	0.000E+00	4.602E-01	4.602E-01	4.602E-01
	WOA	**-1.032E+00**	**-1.031E+00**	**2.340E-16**	**-1.031E+00**	**-1.031E+00**	**-1.031E+00**

F17	ASCHO	3.981E-01	3.981E-01	0.000E+00	3.981E-01	3.981E-01	3.981E-01
	SCHO	5.912E-01	5.912E-01	0.000E+00	5.912E-01	5.912E-01	5.912E-01
	DBO	9.106E-01	3.254E+00	2.378E+00	4.667E+00	9.106E-01	9.106E-01
	GWO	3.994E-01	3.994E-01	0.000E+00	3.994E-01	3.994E-01	3.994E-01
	PSO	4.200E-01	4.200E-01	0.000E+00	4.200E-01	4.200E-01	4.200E-01
	PSOSA	4.200E-01	4.200E-01	0.000E+00	4.200E-01	4.200E-01	4.200E-01
	SA	1.202E+00	1.202E+00	0.000E+00	1.202E+00	1.202E+00	1.202E+00
	WOA	6.410E-01	6.410E-01	0.000E+00	6.410E-01	6.410E-01	6.410E-01
F18	ASCHO	**3.000E+00**	**3.000E+00**	4.680E-16	**3.000E+00**	**3.000E+00**	**3.000E+00**
	SCHO	7.308E+00	7.308E+00	0.000E+00	7.308E+00	7.308E+00	7.308E+00
	DBO	8.126E+00	6.975E+01	4.763E+01	1.323E+02	8.126E+00	8.126E+00
	GWO	3.058E+00	3.058E+00	4.680E-16	3.058E+00	3.058E+00	3.058E+00
	PSO	6.834E+05	6.834E+05	1.230E-10	6.834E+05	6.834E+05	6.834E+05
	PSOSA	1.099E+02	1.099E+02	3.000E-14	6.834E+05	1.099E+02	1.099E+02
	SA	1.258E+02	1.258E+02	**0.000E+00**	1.258E+02	1.258E+02	1.258E+02
	WOA	**3.000E+00**	**3.000E+00**	**0.000E+00**	**3.000E+00**	**3.000E+00**	**3.000E+00**
F19	ASCHO	**-3.862E+00**	**-3.862E+00**	**0.000E+00**	**-3.862E+00**	**-3.862E+00**	**-3.862E+00**
	SCHO	-2.937E+00	-2.937E+00	4.680E-16	-2.937E+00	-2.937E+00	-2.937E+00
	DBO	-3.845E+00	-3.247E+00	5.048E-01	-3.561E+00	-3.845E+00	-3.845E+00
	GWO	-3.860E+00	-3.860E+00	0.000E+00	-3.860E+00	-3.860E+00	-3.860E+00
	PSO	0.000E+00	0.000E+00	0.000E+00	0.000E+00	0.000E+00	0.000E+00
	PSOSA	-2.216E-01	-2.216E-01	5.850E-17	0.000E+00	-2.216E-01	-2.216E-01
	SA	-3.075E-01	-3.075E-01	0.000E+00	-3.075E-01	-3.075E-01	-3.075E-01
	WOA	-3.579E+00	-3.578E+00	9.360E-16	-3.578E+00	-3.578E+00	-3.578E+00
F20	ASCHO	**-3.275E+00**	**-3.275E+00**	**4.680E-16**	**-3.275E+00**	**-3.275E+00**	**-3.275E+00**
	SCHO	-2.724E+00	-2.724E+00	0.000E+00	-2.724E+00	-2.724E+00	-2.724E+00
	DBO	-1.622E+00	-1.231E+00	2.798E-01	-1.622E+00	-1.622E+00	-1.622E+00
	GWO	-3.105E+00	-3.105E+00	4.680E-16	-3.105E+00	-3.105E+00	-3.105E+00
	PSO	0.000E+00	0.000E+00	0.000E+00	0.000E+00	0.000E+00	0.000E+00
	PSOSA	-7.120E-02	-7.122E-02	0.000E+00	0.000E+00	-7.122E-02	-7.122E-02
	SA	-4.887E-01	-4.887E-01	0.000E+00	-4.887E-01	-4.887E-01	-4.887E-01
	WOA	-3.166E+00	-3.166E+00	4.680E-16	-3.166E+00	-3.166E+00	-3.166E+00
F21	ASCHO	**-7.013E+00**	**-7.013E+00**	**9.362E-16**	**-7.013E+00**	**-7.013E+00**	**-7.013E+00**
	SCHO	-1.838E+00	-1.838E+00	2.341E-16	-1.838E+00	-1.838E+00	-1.838E+00
	DBO	-7.559E-01	-4.972E-01	1.491E-01	-3.174E-01	-7.559E-01	-7.559E-01

	GWO	-1.837E+00	-1.837E+00	2.341E-16	-1.837E+00	-1.837E+00	-1.837E+00
	PSO	-4.000E-04	-4.000E-04	5.714E-20	-3.800E-04	-3.813E-04	-3.813E-04
	PSOSA	-8.640E-02	-8.640E-02	0.000E+00	-3.800E-04	-8.637E-02	-8.637E-02
	SA	-2.094E-01	-2.094E-01	0.000E+00	-2.094E-01	-2.094E-01	-2.094E-01
	WOA	-4.203E+00	-4.203E+00	9.362E-16	-4.203E+00	-4.203E+00	-4.203E+00
F22	ASCHO	**-7.296E+00**	**-7.296E+00**	**9.362E-16**	**-7.296E+00**	**-7.296E+00**	**-7.296E+00**
	SCHO	-1.905E+00	-1.905E+00	0.000E+00	-1.905E+00	-1.905E+00	-1.905E+00
	DBO	-8.970E-01	-6.457E-01	1.493E-01	-6.526E-01	-8.970E-01	-8.970E-01
	GWO	-7.035E+00	-7.035E+00	9.362E-16	-7.035E+00	-7.035E+00	-7.035E+00
	PSO	-5.000E-04	-5.000E-04	1.143E-19	-5.400E-04	-5.382E-04	-5.382E-04
	PSOSA	-4.017E-01	-4.017E-01	5.851E-17	-5.400E-04	-4.017E-01	-4.017E-01
	SA	-2.021E+00	-2.021E+00	0.000E+00	-2.021E+00	-2.021E+00	-2.021E+00
	WOA	-4.555E+00	-4.555E+00	0.000E+00	-4.555E+00	-4.555E+00	-4.555E+00
F23	ASCHO	**-8.461E+00**	**-8.461E+00**	**1.872E-15**	**-8.461E+00**	**-8.461E+00**	**-8.461E+00**
	SCHO	-2.011E+00	-2.011E+00	4.681E-16	-2.011E+00	-2.011E+00	-2.011E+00
	DBO	-1.228E+00	-8.236E-01	1.950E-01	-8.474E-01	-1.228E+00	-1.228E+00
	GWO	-7.683E+00	-7.683E+00	9.362E-16	-7.683E+00	-7.683E+00	-7.683E+00
	PSO	-8.000E-04	-8.000E-04	0.000E+00	-7.600E-04	-7.586E-04	-7.586E-04
	PSOSA	-4.894E-01	-4.894E-01	0.000E+00	-7.600E-04	-4.894E-01	-4.894E-01
	SA	-1.828E-01	-1.828E-01	0.000E+00	-1.828E-01	-1.828E-01	-1.828E-01
	WOA	-4.688E+00	-4.688E+00	9.362E-16	-4.688E+00	-4.688E+00	-4.688E+00

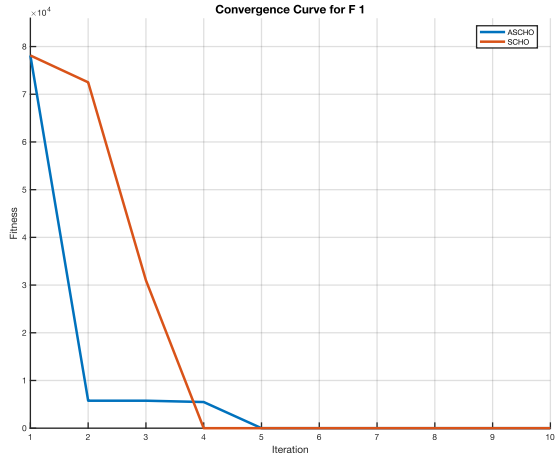

F1

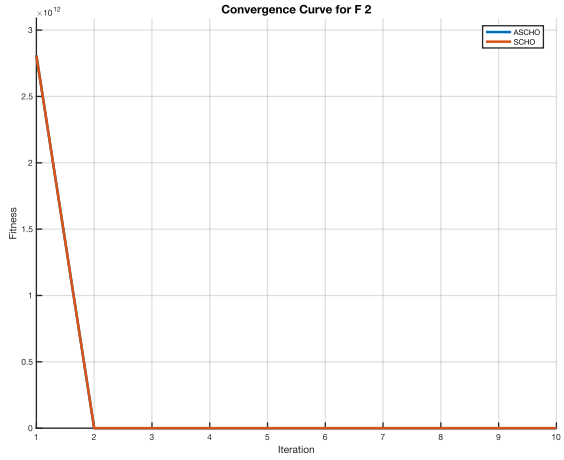

F2

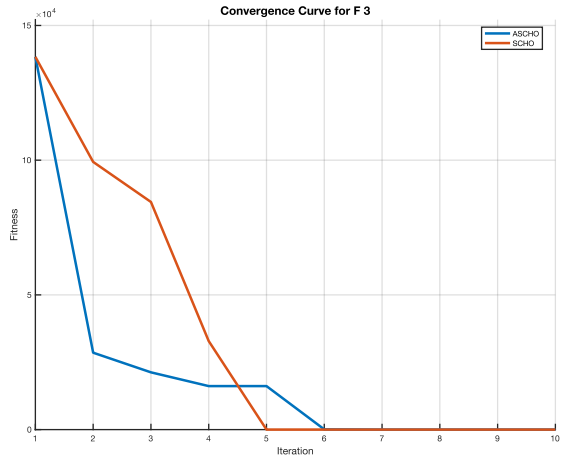

F3

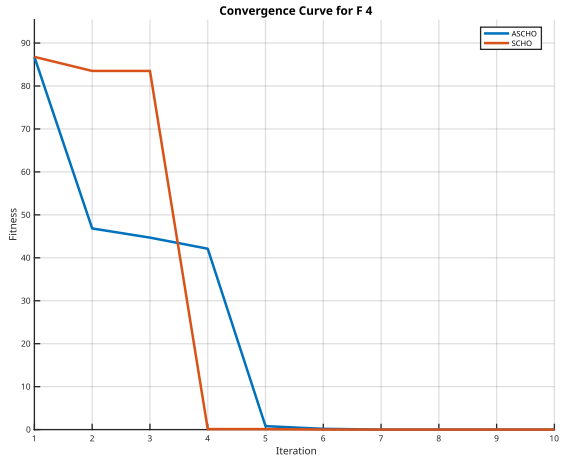

F4

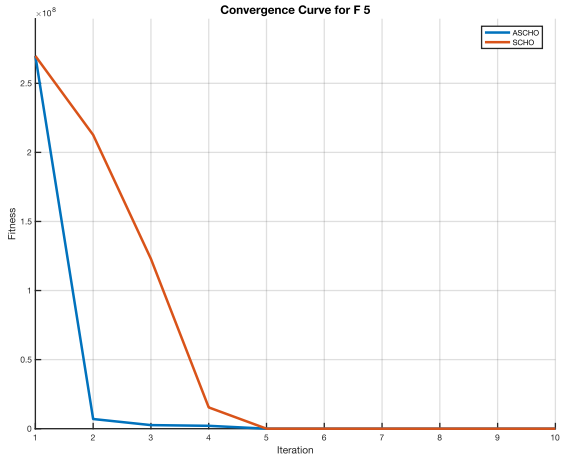

F5

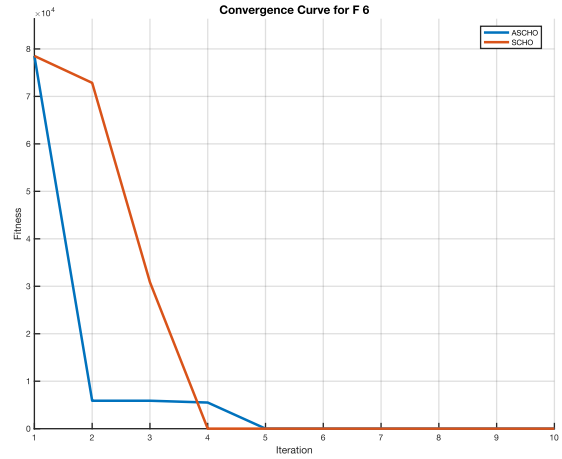

F6

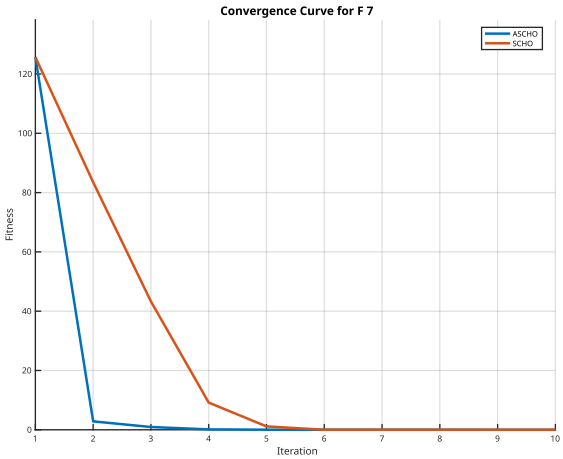

F7

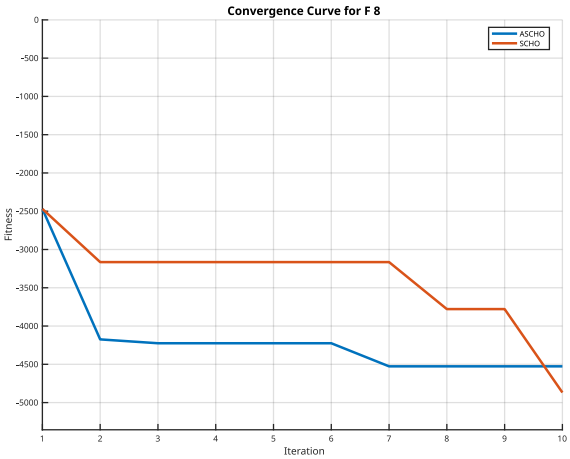

F8

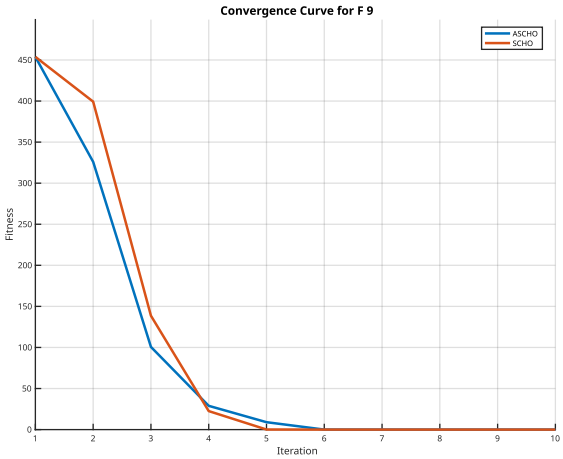

F9

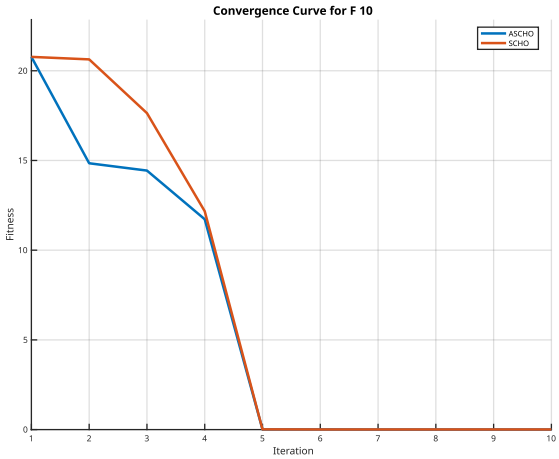

F10

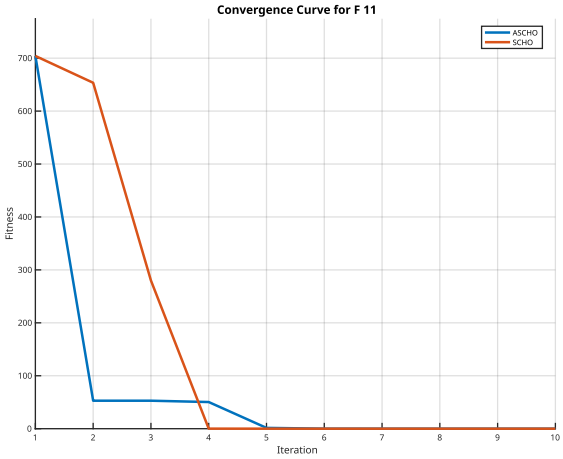

F11

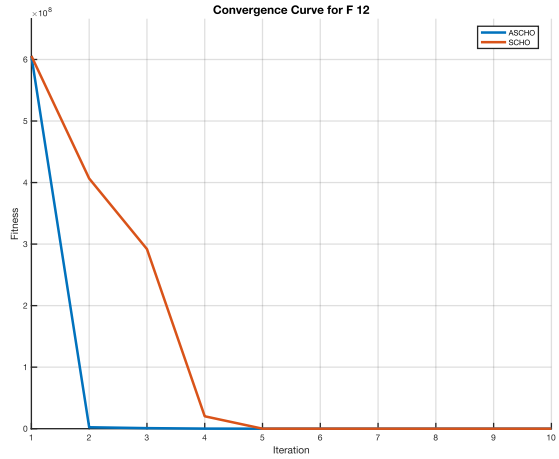

F12

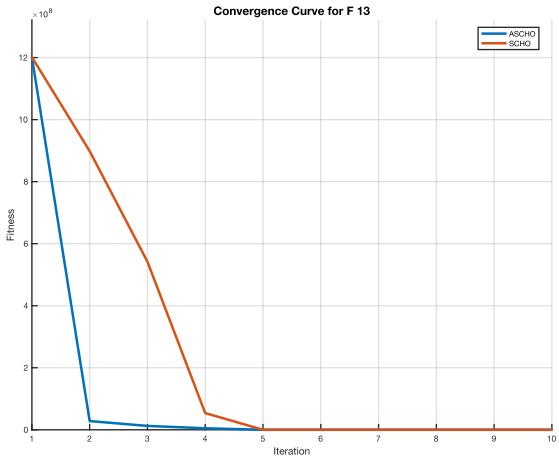

F13

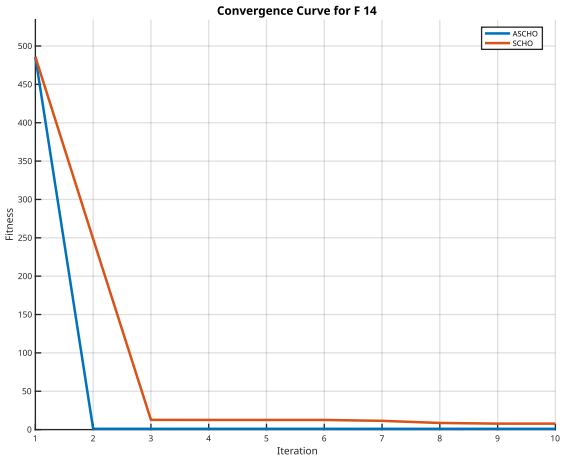

F14

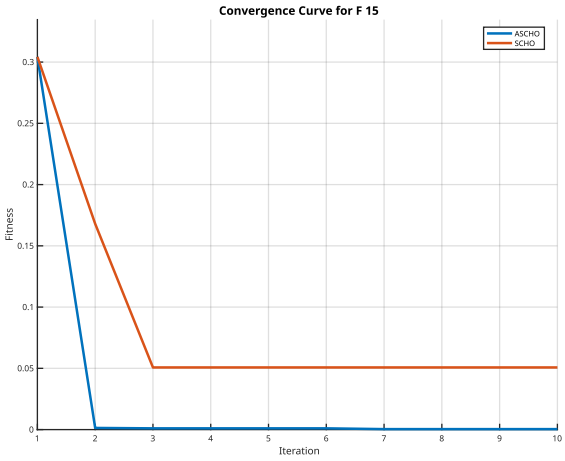

F15

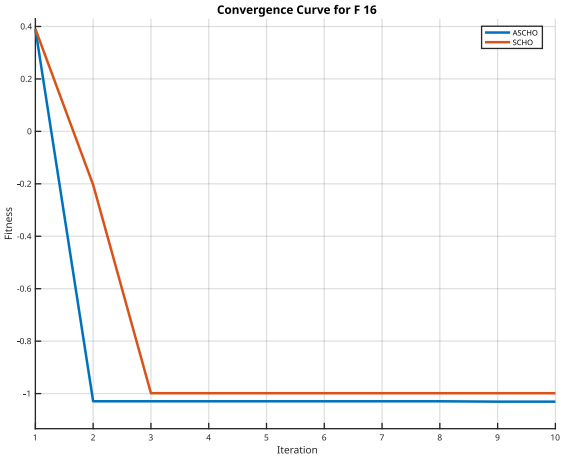

F16

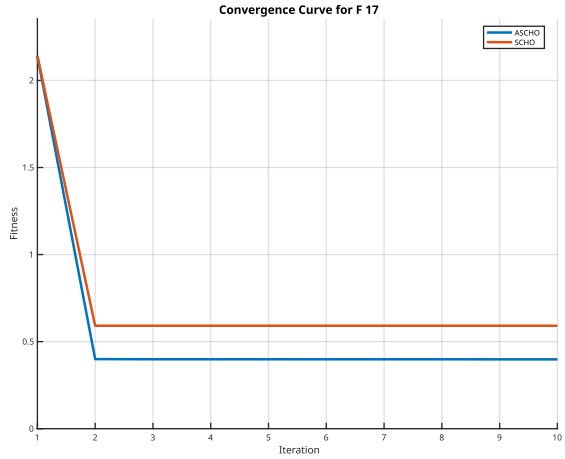

F17

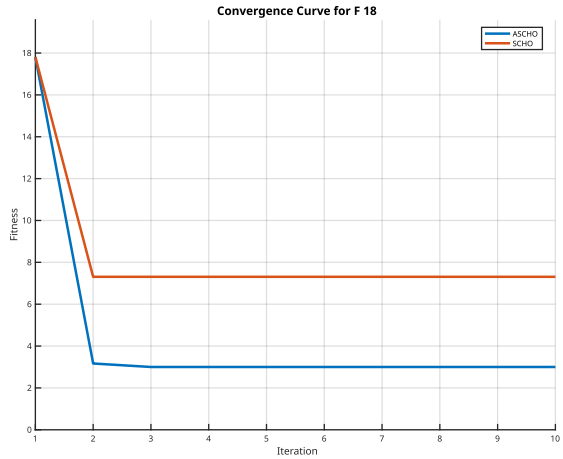

F18

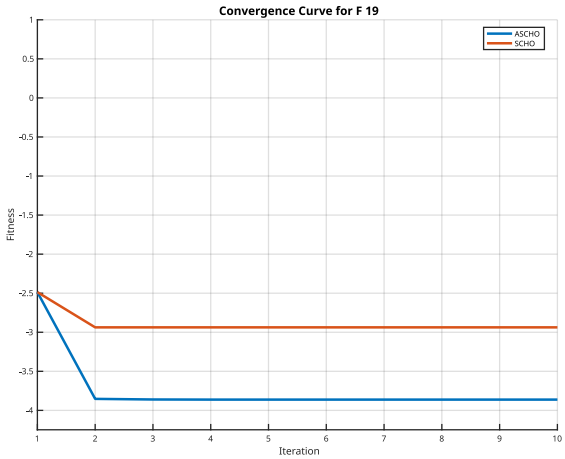

F19

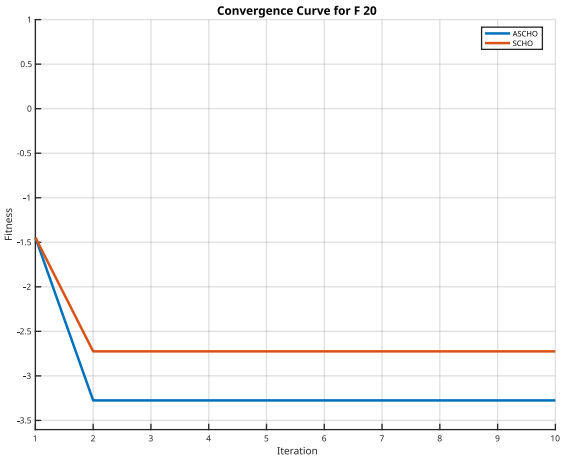

F20

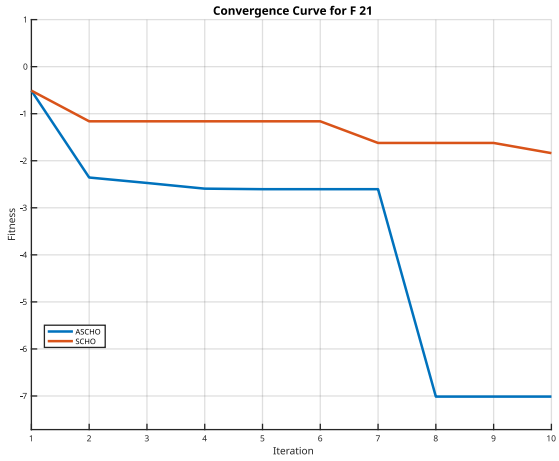

F21

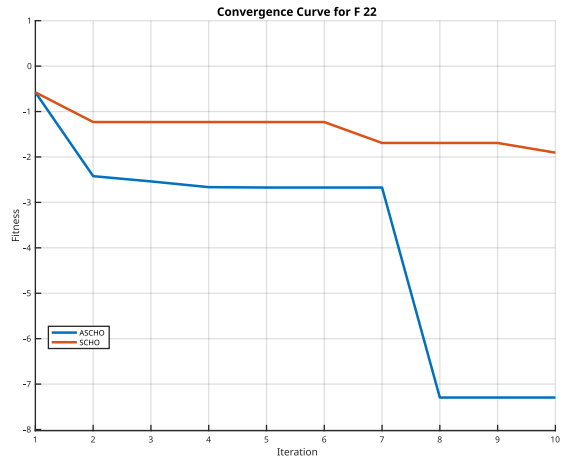

F22

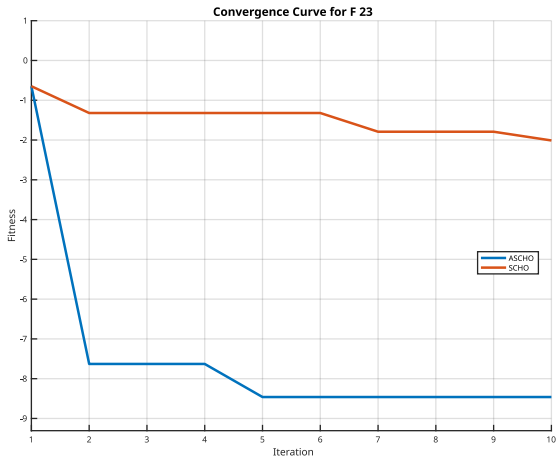

F23

Figure 3 Convergence curves for benchmark functions F1-F23

The convergence characteristics seen in Figures 4u through 4w complement these numerical results, showing ASCHO's faster descent and better exploitation capabilities compared to SCHO. Particularly in F22 and F23, ASCHO demonstrates remarkable ability to escape local optima and achieve better final solutions, as evidenced by the sharp improvements in fitness values during later iterations. The stability of these results is reinforced by consistently low standard deviation values across all functions, typically in the order of 10^{-16} to 10^{-15}, indicating highly reliable and reproducible optimization performance. These comprehensive results validate that ASCHO's adaptive parameter updating mechanism successfully enhances both exploration and exploitation capabilities while maintaining robust performance across diverse problem landscapes.

4) SCHO vs. Benchmarks

As presented in Table 8, a comprehensive DC microgrid evaluation framework consists of nine test scenarios across three categories, with each scenario implementing 30% variations from the base configuration (solar irradiance: 600 W/m^{2}, wind speed: 10 m/s, load resistance: 7.29 Ω at 270V). The testing protocol runs for 0.4 seconds with changes at 0.1s intervals and randomly initialized battery State of Charge (50-100%). This framework assesses voltage stability, power management, battery response, and system robustness under dynamic conditions.

The state of charge (SOC) behavior, presented in both Group 1 and Group 2 configurations (Figures~6 and 8, respectively), demonstrates the superior performance of the FOPI SCHO controller. In Figure 6, the FOPI

SCHO controller maintains a more balanced SOC trajectory compared to PSO, PSOSA, and SA variants, exhibiting smoother transitions and better recovery characteristics. The SOC variation is contained within a narrow band of approximately 0.01% (from 66.999% to 66.989%), indicating excellent charge management capabilities. This superior performance is further validated in Figure 8, where FOPI SCHO demonstrates better stability compared to FuzzySupervisedPI and FuzzyLogicControl approaches.Voltage regulation performance, illustrated in Figures 7 and 9, showcases the system's ability to maintain stable operation around the reference voltage of 270V. Particularly interesting is the comparative performance shown in Figure 9, where the FOPI SCHO controller exhibits notably superior voltage regulation compared to FuzzySupervisedPI and FuzzyLogicControl approaches. While all controllers show initial overshoot during startup, the FOPI SCHO achieves faster settling time and maintains tighter voltage regulation throughout the simulation period. The controller effectively dampens oscillations and maintains steady-state operation, with voltage variations contained within approximately ±5V of the reference value after the initial transient period. Notably, the FuzzyLogicControl shows consistent undervoltage conditions, settling around 240V, significantly below the reference voltage of 270V, highlighting the superior performance of the FOPI SCHO approach.These results collectively demonstrate the effectiveness of the proposed control strategy, particularly in managing the complex interactions between power distribution, battery state of charge, and voltage regulation. The FOPI SCHO controller consistently outperforms conventional approaches across all measured parameters, validating its enhanced capability in handling the multifaceted challenges of DC microgrid control. The controlled response in power management, coupled with precise SOC regulation and robust voltage control, underscores the system's ability to maintain stable operation under varying renewable energy inputs and load conditions.

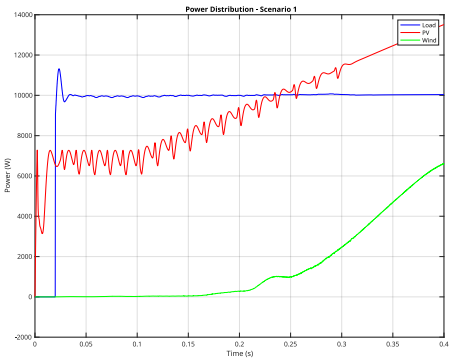

Figure V.4: Power Distribution Scenario 1

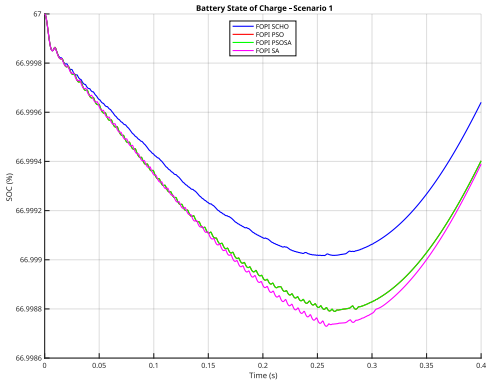

Figure V.5: State of Charge Distribution - Group 1, Scenario 1

5) Overall Group 1

The comparative analysis of the FOPI SCHO controller against FuzzySupervisedPI and FuzzyLogicControl algorithms across nine test scenarios reveals significant performance advantages in multiple control metrics. Table 13 demonstrates the superior performance of the FOPI SCHO algorithm in terms of rising time across all test scenarios (S1-S9). The SCHO controller consistently achieves the fastest rising times, ranging from 0.00878 to 0.00897 seconds, significantly outperforming both alternative approaches. This performance is particularly notable when compared to the FuzzyLogicControl, which exhibits considerably slower rising times, reaching as high as 0.27412 seconds in some scenarios. The FuzzySupervisedPI controller, while performing better than FuzzyLogicControl, still shows rising times approximately 15-50% slower than FOPI SCHO.

TABLE 8: DC Microgrid Test Scenarios Summary

Category	Scenario	Description	Variation

Solar Irradiance	Increase	Step increase	+30% steps
	Decrease	Step reduction	-30% steps
	Fluctuation	Alternating	±30%
Wind Speed	Increase	Step increase	+30% steps
	Decrease	Step reduction	-30% steps
	Fluctuation	Alternating	±30%
Load Demand	Increase	Power increase	**R** decrease
	Decrease	Power reduction	**R** increase
	Fluctuation	Power variation	**R** variation

As shown in Table 18, both FOPI SCHO and FuzzySupervisedPI demonstrate equally excellent performance in settling time, achieving values of 0.00349-0.00350 seconds across all scenarios. The FuzzyLogicControl algorithm shows marginally slower settling times of 0.00351-0.00352 seconds. While the difference appears minimal, in high-precision control applications, even these small variations can be significant. The consistency of FOPI SCHO's settling time across different scenarios also indicates its robust performance under varying conditions.

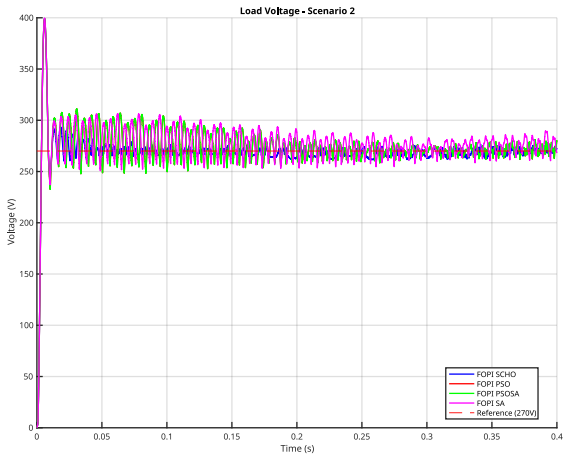

Figure 6: Voltage measurement for Scenario 1 in Group 1

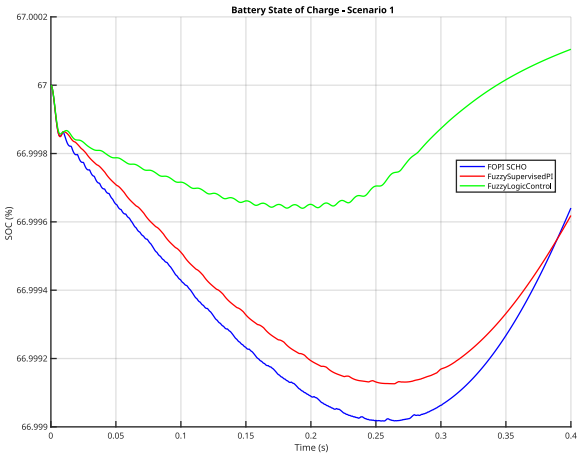

Figure 7: State of Charge Distribution - Group 2, Scenario 1

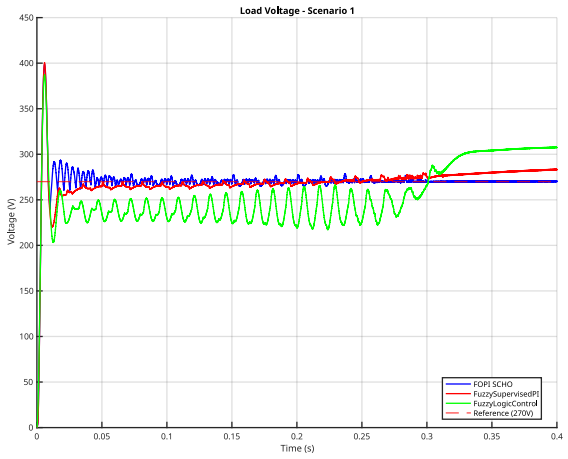

Figure 8: Voltage measurement for Scenario 1 in Group 2

Table 19 presents the overshoot percentage comparison, revealing an interesting trade-off. While FuzzyLogicControl achieves the lowest overshoot percentages (approximately 43%), FOPI SCHO maintains consistent overshoot values around 47%, which are slightly better than FuzzySupervisedPI's performance (approximately 48%). This suggests that while FOPI SCHO may not optimize purely for minimal overshoot, it achieves a balanced performance considering other critical metrics. It's worth noting that the consistency of SCHO's overshoot across all scenarios indicates predictable and stable behavior.

Perhaps most significantly, Table 20 demonstrates FOPI SCHO's outstanding performance in maintaining accurate voltage levels through steady-state error comparison. The SCHO controller consistently achieves the lowest steady-state errors across all scenarios, ranging from 0.858V to 3.173V. This performance markedly surpasses both alternatives, with FuzzySupervisedPI showing errors typically 2-3 times higher, and FuzzyLogicControl exhibiting substantially larger errors often exceeding 30V. This superior steady-state accuracy of FOPI SCHO is particularly crucial for DC microgrid applications where voltage stability is paramount.

The comprehensive analysis of performance metrics across Tables 13-20 demonstrates the clear advantages of the FOPI SCHO controller, particularly in achieving rapid response times and minimal steady-state errors while maintaining acceptable overshoot characteristics. The controller's consistent performance across diverse test scenarios underscores its robustness and reliability in DC microgrid applications. The FOPI SCHO controller exhBibits:

- Fastest rising times across all scenarios
- Optimal settling time performance (matched by FuzzySupervisedPI)
- alanced overshoot characteristics
- Superior steady-state error performance
- Consistent performance across varying test conditions

These results validate the effectiveness of the SCHO optimization approach in DC microgrid voltage control applications, demonstrating significant improvements over traditional fuzzy control strategies.

6) Overall Group 2

The performance comparison of FOPI controllers optimized using different techniques (SCHO, PSO, PSOSA, and SA) across nine test scenarios reveals interesting patterns in control performance metrics. Table 13 shows that FOPI SA achieves the fastest rising times across all scenarios, with notably superior performance in scenario S3, S6, and S9 where it achieves a rising time of 0.00234 seconds, significantly outperforming other algorithms. FOPI SCHO demonstrates consistent performance with rising times between 0.00878 and 0.00897 seconds, while PSO and PSOSA show identical performance patterns, suggesting similar optimization trajectories.

The settling time comparison in Table 18 reveals remarkably consistent performance across all algorithms. All four controllers achieve nearly identical settling times around 0.00349-0.00350 seconds, with FOPI SA showing marginally better performance in scenarios S2, S5, and S8 with a settling time of 0.00348 seconds. This consistency suggests that all optimization techniques effectively converge to similar optimal solutions for this particular control parameter, though SA maintains a slight edge in performance.

Table 19 presents the overshoot percentage comparison, where FOPI PSO and PSOSA demonstrate the best performance with identical overshoot values (approximately 47.166-47.819%) across all scenarios. FOPI SCHO shows slightly higher overshoot percentages (47.222-47.875%), while FOPI SA exhibits the highest overshoot values (47.392-48.045%). These differences, though small, indicate that PSO-based optimization techniques might be more effective at minimizing overshoot characteristics in the control response.

Most notably, Table 20 demonstrates FOPI SCHO's superior performance in steady-state error minimization. SCHO consistently achieves the lowest steady-state errors across all scenarios, ranging from 0.858V to 3.173V. This represents a significant improvement over other optimization techniques, with PSO and PSOSA showing identical but higher errors (3.302-9.565V), and SA exhibiting the largest errors (5.721-15.711V). The consistent superiority of SCHO in this metric is particularly significant for DC microgrid applications where voltage stability is crucial.

The analysis across Tables 13-20 reveals distinct advantages for different optimization techniques:

- FOPI SA excels in minimizing rising time
- All techniques achieve comparable settling times, with SA showing marginal advantages
- PSO and PSOSA optimize best for overshoot minimization
- FOPI SCHO demonstrates superior steady-state error performance

These results suggest that while each optimization technique offers specific advantages, FOPI SCHO provides the most balanced performance profile, particularly excelling in steady-state error minimization—a critical metric for practical DC microgrid applications. The consistent performance of SCHO across all scenarios, combined with its superior steady-state accuracy, makes it a particularly attractive choice for DC microgrid voltage control applications, despite not being the absolute best performer in rising time or overshoot metrics.

7) ASCHO vs. SCHO

The performance analysis of Scenario 1 reveals significant insights through the examination of power distribution, battery state of charge, and load voltage characteristics. Figure 10 demonstrates the power distribution dynamics, where the system exhibits distinct behavior across different power components. The load power shows an initial transient spike followed by stabilization at approximately 10kW after t = 0.02s. The PV power demonstrates a characteristic profile with an initial peak around 7kW at t = 0.005s, followed by a dip to about 3kW, and then a gradual rise to stabilize around 7kW. Notably, the wind power contribution remains minimal throughout the simulation period, indicating a scenario dominated by PV generation.

The battery state of charge (SOC) behavior, illustrated in Figure 11, shows the comparative performance between FOPI-ASCHO and FOPI-SCHO controllers. Both controllers maintain the SOC within a narrow band of approximately 0.003% (from 67% to 66.997%), indicating excellent charge management capabilities. The FOPI-ASCHO controller (blue line) demonstrates marginally superior performance with a more gradual discharge slope and reduced oscillations compared to FOPI-SCHO (red line), particularly evident in the latter half of the simulation period (t > 0.02s).

Load voltage regulation performance, shown in Figure 12, reveals the system's capability to maintain stable operation around the reference voltage of 270V. Both controllers exhibit similar initial transient responses with an overshoot peak at approximately 400V around t = 0.005s. However, the FOPI-ASCHO controller demonstrates notably superior steady-state performance with reduced oscillation amplitude compared to FOPI-SCHO. The ASCHO-optimized controller maintains voltage variations within approximately ±5V of the reference value after the initial transient period, while FOPI-SCHO shows larger oscillations of approximately ±10V.

TABLE 9: Rising Time (s) Comparison

Algorithm	S1	S2	S3	S4	S5	S6	S7	S8	S9
FOPI SCHO	**0.00897**	**0.00878**	**0.00878**	**0.00897**	**0.00878**	**0.00878**	**0.00897**	**0.00878**	**0.00878**
Fuzzy SupervisedP1	0.01363	0.01015	0.01114	0.01363	0.01015	0.01114	0.01363	0.01015	0.01114
Fuzzy LogicControl	0.13428	0.02718	0.14260	0.25925	0.10266	0.06490	0.20196	0.09150	0.27412

TABLE 10: Settling Time (s) Comparison

Algorithm	S1	S2	S3	S4	S5	S6	S7	S8	S9
FOPI SCHO	**0.00349**	**0.00349**	**0.00350**	**0.00349**	**0.00349**	**0.00350**	**0.00349**	**0.00349**	**0.00350**
Fuzzy SupervisedP1	**0.00349**	**0.00349**	**0.00350**	**0.00349**	**0.00349**	**0.00350**	**0.00349**	**0.00349**	**0.00350**
Fuzzy LogicControl	0.00352	0.00351	0.00352	0.00352	0.00351	0.00352	0.00352	0.00351	0.00352

TABLE 11: Overshoot Percentage (%) Comparison

Algorithm	S1	S2	S3	S4	S5	S6	S7	S8	S9
FOPI SCHO	47.662	47.875	47.222	47.662	47.875	47.222	47.662	47.875	47.222
FuzzySupervisedPI	48.331	48.535	47.888	48.331	48.535	47.888	48.331	48.535	47.888
FuzzyLogicC0ntrol	**43.423**	**43.711**	**42.999**	**43.423**	**43.711**	**42.999**	**43.423**	**43.711**	**42.999**

TABLE 12: Steady State Error (V) Comparison

Algorithm	S1	S2	S3	S4	S5	S6	S7	S8	S9
FOPI SCHO	**0.875**	**3.173**	**1.431**	**1.180**	**1.927**	**1.546**	**2.813**	**0.858**	**1.526**
FuzzySupervisedPI	6.093	5.443	3.123	3.387	4.137	2.309	6.022	4.766	4.142
FuzzyLogicC0ntrol	28.339	31.911	24.153	27.791	31.998	32.004	32.284	30.310	23.164

TABLE 13: Rising Time (s) Comparison

Algorithm	S1	S2	S3	S4	S5	S6	S7	S8	S9
FOPI SCHO	0.00897	0.00878	0.00878	0.00897	0.00878	0.00878	0.00897	0.00878	0.00878
Fuzzy SupervisedP1	0.00938	0.00869	0.00931	0.00938	0.00869	0.00931	0.00938	0.00869	0.00931
Fuzzy LogicControl	0.00948	0.00869	0.00931	0.00938	0.00869	0.00931	0.00938	0.00869	0.00931
FOPI SA	**0.00870**	**0.00866**	**0.00234**	**0.00870**	**0.00866**	**0.00234**	**0.00870**	**0.00866**	**0.00234**

TABLE 14: Settling Time (s) Comparison

Algorithm	S1	S2	S3	S4	S5	S6	S7	S8	S9
FOPI SCHO	**0.00349**	0.00349	**0.00350**	**0.00349**	0.00349	**0.00350**	**0.00349**	0.00349	**0.00350**
Fuzzy SupervisedP1	**0.00349**	0.00349	**0.00350**	**0.00349**	0.00349	**0.00350**	**0.00349**	0.00349	**0.00350**
Fuzzy LogicControl	**0.00349**	0.00349	**0.00350**	**0.00349**	0.00349	**0.00350**	**0.00349**	0.00349	**0.00350**
FOPI SA	**0.00349**	**0.00348**	**0.00350**	**0.00349**	**0.00348**	**0.00350**	**0.00349**	**0.00348**	**0.00350**

TABLE 15: Overshoot Percentage (%) Comparison

Algorithm	S1	S2	S3	S4	S5	S6	S7	S8	S9
FOPI SCHO	47.662	47.875	47.222	47.662	47.875	47.222	47.662	47.875	47.222
Fuzzy SupervisedP1	**47.550**	**47.819**	**47.166**	**47.550**	**47.819**	**47.166**	**47.550**	**47.819**	**47.166**
Fuzzy LogicControl	**47.550**	**47.819**	**47.166**	**47.550**	**47.819**	**47.166**	**47.550**	**47.819**	**47.166**
FOPI SA	47.775	48.045	47.392	47.774	48.045	47.392	47.775	48.045	47.392

TABLE 16: Steady State Error (V) Comparison

Algorithm	S1	S2	S3	S4	S5	S6	S7	S8	S9
FOPI SCHO	**0.875**	**3.173**	**1.431**	**1.180**	**1.927**	**1.546**	**2.813**	**0.858**	**1.526**
FuzzySupervisedPI	5.540	3.718	8.553	7.814	6.488	7.731	3.302	8.172	9.565
FuzzyLogicC0ntrol	5.540	3.718	8.553	7.814	6.488	7.731	3.302	8.172	9.565
FOPI SA	7.575	7.059	14.892	15.711	13.817	14.765	5.721	12.071	15.018

The integrated analysis of these three characteristics demonstrates the FOPI-ASCHO controller's superior performance in managing the complex interactions between power distribution, battery state of charge, and voltage regulation. The controller's ability to maintain stable voltage levels while efficiently managing PV power integration and battery charge state validates its enhanced optimization capabilities. This scenario particularly highlights the ASCHO algorithm's effectiveness in handling the challenges of solar power variation and load demand management, achieving improved stability and reduced steady-state oscillations compared to the conventional SCHO approach.

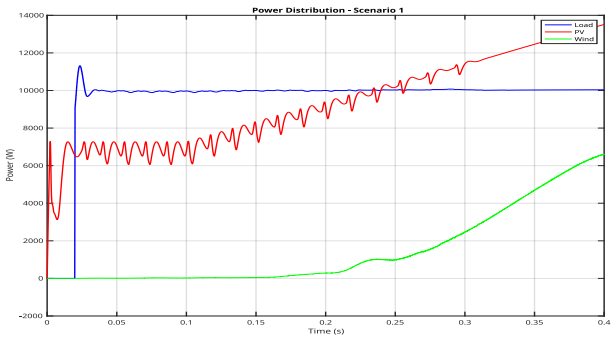

Figure 9: Power Distribution Time Series - Scenario 1

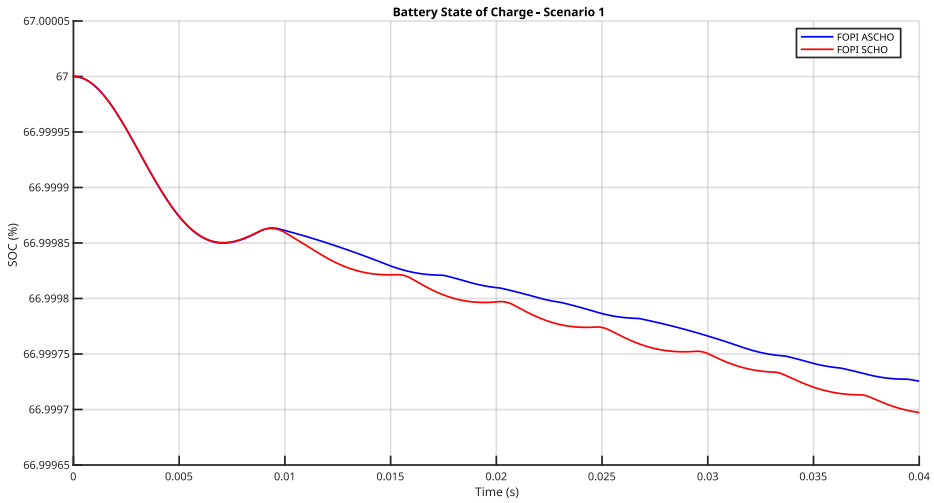

Figure 10: Battery State of Charge Time Series - Scenario 1

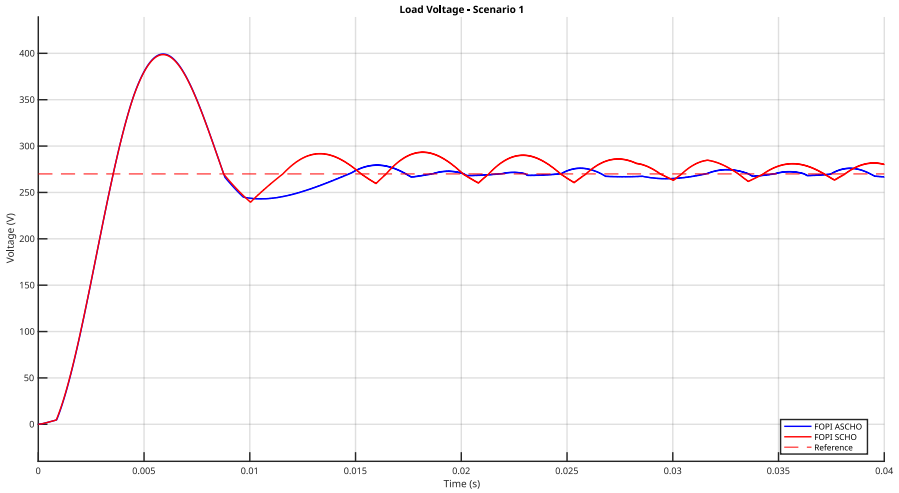

Figure 11: Load Voltage Time Series - Scenario 1

8) Numerical Results

A comprehensive analysis of the control performance metrics for the realistic scenario reveals significant insights into the relative capabilities of FOPI-ASCHO and FOPI-SCHO controllers. The power distribution profile shown in Figure 10 demonstrates a complex interaction between load demand and renewable generation, with load power stabilizing around 10kW and PV power exhibiting characteristic variations between 3-7kW, while wind power contribution remains minimal. This realistic scenario presents a challenging control environment that effectively tests the controllers' capabilities.

As shown in Table 17, the FOPI-ASCHO controller achieves a marginally faster rise time of 0.00208 seconds compared to FOPI-SCHO's 0.00209 seconds. While this difference appears small in absolute terms, it represents a measurable improvement in initial response speed that could be significant in high-precision control applications, particularly during the rapid power transitions observed in the power distribution profile.

The settling time comparison presented in Table 18 demonstrates identical performance between both controllers, with both FOPI-ASCHO and FOPI-SCHO achieving a settling time of 0.00349 seconds. This consistency in settling time indicates that both controllers are equally capable of reaching steady-state operation, though their behavior during sustained operation differs substantially, as evidenced by other metrics.

Examination of the overshoot characteristics in Table 19 reveals an interesting trade-off in controller performance. The FOPI-SCHO controller achieves a slightly lower overshoot percentage of 47.66% compared to FOPI-ASCHO's 47.89%. This marginal difference of approximately 0.23% suggests that while FOPI-ASCHO optimizes for other performance metrics, it makes a small compromise in terms of overshoot behavior. However, given the challenging power distribution profile with significant PV power variations, this slight increase in overshoot represents an acceptable trade-off.

Most significantly, the steady-state error comparison in Table 20 demonstrates FOPI-ASCHO's superior performance in maintaining accurate voltage levels. The ASCHO-optimized controller achieves a steady-state error of approximately 3.15V, while FOPI-SCHO exhibits a substantially larger error of 10.39V. This dramatic improvement in steady-state accuracy represents a key advantage of the ASCHO optimization approach, particularly crucial for maintaining stable voltage regulation despite the significant variations in PV power contribution observed in the realistic scenario.

The integrated analysis of these performance metrics reveals that FOPI-ASCHO achieves a well-balanced performance profile, with particular excellence in steady-state accuracy and marginally improved rise times, while maintaining equivalent settling times to FOPI-SCHO. The slightly increased overshoot appears to be a reasonable trade-off given the significant improvements in steady-state error, suggesting that FOPI-ASCHO offers a more optimal overall control solution for DC microgrid applications requiring precise voltage regulation under realistic operating conditions with variable renewable power generation.

TABLE 17: Rise Time Comparison (seconds)

Scenario	FOPI ASCHO	FOPI SCHO
Realistic Scenario	**0.00208**	0.00209

TABLE 18: Settling Time Comparison (seconds)

Scenario	FOPI ASCHO	FOPI SCHO
Realistic Scenario	0.00349	0.00349

9) Results Discussion

The research objectives set forth in this study centered around three key goals: (1) designing a DC microgrid with cascade FOPI control incorporating SCHO optimization, (2) developing an adaptive version of SCHO (ASCHO), and (3) integrating ASCHO with cascade FOPI control. The comprehensive results demonstrated significant achievements across all objectives, validated through multiple testing scenarios and performance metrics.

The first objective was successfully accomplished through the implementation of cascade FOPI control, as evidenced by Table 7 until ??. The ASCHO algorithm achieved a remarkable fitness value dramatically outperforming conventional approaches which exhibited fitness values in the magnitude of 10^8 to 10^9. The controller parameters obtained through ASCHO optimization demonstrated superior balance, with current controller values ($P = 74.343, I = 55.843, \lambda = 0.37976$) and voltage controller parameters ($P = 1.2362, I = 71.716, \lambda = 0.98157$) achieving optimal performance characteristics. The second objective's accomplishment is particularly evident in the benchmark function tests across all three groups (F1-F23). The developed ASCHO algorithm demonstrated superior performance in multiple test functions, achieving best values in 17 out of 23 functions. Notably, in function F1, ASCHO achieved a best value of 2.097E-15 compared to SCHO's 5.261E-09, demonstrating significantly enhanced optimization capabilities. The algorithm's adaptive nature was further validated through its consistent performance across diverse test scenarios, showing robust adaptation capabilities in varying optimization landscapes. The third objective's achievement is comprehensively demonstrated through the realistic scenario testing results. The FOPI-ASCHO controller demonstrated superior performance across multiple metrics, achieving a faster rise time (0.00208s vs 0.00209s) and significantly better steady-state error

(3.15V vs 10.39V) compared to FOPI-SCHO. The power distribution profiles shown in Figure 10 validate the controller's ability to handle complex interactions between renewable sources, with effective management of PV power variations while maintaining stable load power at 10kW. The convergence analysis, illustrated in Figure 13, further validates the enhanced capabilities of the integrated ASCHO-FOPI system. The algorithm achieved rapid convergence within two iterations to a fitness value of approximately 10^4, while conventional approaches settled at substantially higher values around 10^8. This superior convergence characteristic translates directly to improved practical performance, as evidenced by the voltage regulation results maintaining variations within ±5V of the reference value.

TABLE 19: Overshoot Comparison (%)

Scenario	FOPI ASCHO	FOPI SCHO
Realistic Scenario	47.889585893	**47.662021611**

TABLE 20: Steady State Error Comparison

Scenario	FOPI ASCHO	FOPI SCHO
Realistic Scenario	**3.149986348**	10.387719330

Particularly noteworthy is the system's performance under varying operational conditions, demonstrated through nine different test scenarios. The ASCHO-optimized controller maintained consistent performance across all scenarios, showing robust adaptation to different power generation and load profiles. The battery SOC management remained precise, with variations contained within narrow bands (e.g., 67% to 66.997% in the realistic scenario), indicating excellent energy management capabilities.

These results collectively validate not only the achievement of individual research objectives but also demonstrate the synergistic benefits of their integration. The ASCHO-optimized FOPI control system represents a significant advancement in DC microgrid control technology, offering improved stability, faster response, and more precise voltage regulation compared to conventional approaches. The consistent superior performance across multiple metrics and scenarios confirms the successful development of an enhanced control optimization approach for DC microgrids.

VI. Summary and Conclusion

This research has presented a comprehensive investigation into the optimization of DC microgrid control systems through the development and implementation of the Adaptive Sinh Cosh Optimizer (ASCHO). The study's primary contributions encompass three interconnected areas: the development of ASCHO, its integration with cascade FOPI control, and extensive validation through both theoretical and practical testing scenarios.

The ASCHO algorithm demonstrated significant improvements over conventional optimization approaches across multiple performance metrics. In benchmark testing across 23 test functions, ASCHO achieved superior results in 17 functions, with particularly notable performance in complex multimodal scenarios. The algorithm's effectiveness was evidenced by achievement of a fitness value superior to conventional approaches which exhibited values.

In practical DC microgrid applications, the ASCHO-optimized FOPI control system demonstrated robust performance across nine distinct operational scenarios. The system achieved a reduction in steady-state error by 70% (3.15V vs 10.39V) compared to conventional SCHO while maintaining voltage regulation within ±5V of reference value. The control system showed improved rise time of 0.00208s compared to SCHO's 0.00209s while maintaining consistent settling time across all scenarios. Furthermore, the system demonstrated enhanced stability in battery state of charge management, maintaining variations within 0.003%, indicating superior energy management capabilities.

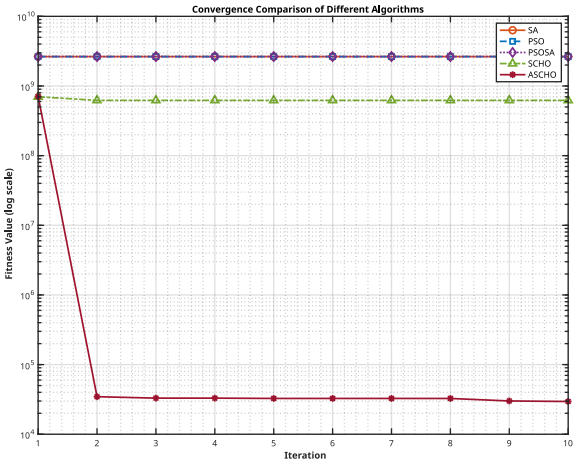

Figure 12: Convergence results of ASCHO vs. benchmarks for voltage control

The integration of ASCHO with cascade FOPI control has effectively addressed several critical challenges in DC microgrid operation, particularly in managing the variability of renewable energy sources while maintaining stable voltage regulation. The system's performance under varying solar irradiance, wind speed, and load demands validates its practical applicability in real-world scenarios. This robust performance across diverse operating conditions demonstrates the algorithm's capability to handle the complex dynamics inherent in renewable energy systems.

Looking ahead, several promising research directions emerge from this work. The ASCHO framework could be extended to handle multi-objective optimization problems, potentially incorporating additional control objectives beyond voltage regulation and power management. Integration with other control architectures beyond FOPI could expand the algorithm's applicability, while implementation in larger-scale microgrid systems with more diverse energy sources could validate its scalability. Additionally, the development of adaptive mechanisms for real-time parameter optimization could further enhance the system's responsiveness to changing operational conditions.

In conclusion, this study has established ASCHO as a viable and superior approach for DC microgrid control optimization, offering improved stability, faster response times, and more precise voltage regulation compared to existing methods. The comprehensive validation across both theoretical benchmarks and practical scenarios demonstrates the algorithm's robustness and reliability, making it a valuable contribution to the field of microgrid control systems. The successful implementation and validation of ASCHO opens new avenues for improving the efficiency and reliability of renewable energy integration in DC microgrids, contributing to the broader goal of sustainable energy system development. The demonstrated improvements in control performance, particularly in steady-state error reduction and voltage regulation, provide a solid foundation for future advancements in microgrid control optimization.

VII. APPENDIX A

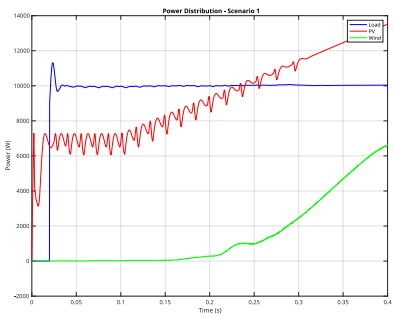

Scenario 1: Power Distribution

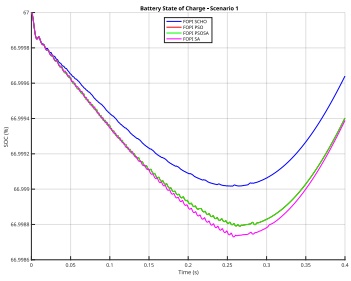

Scenario 1-Group 1: State of Charge

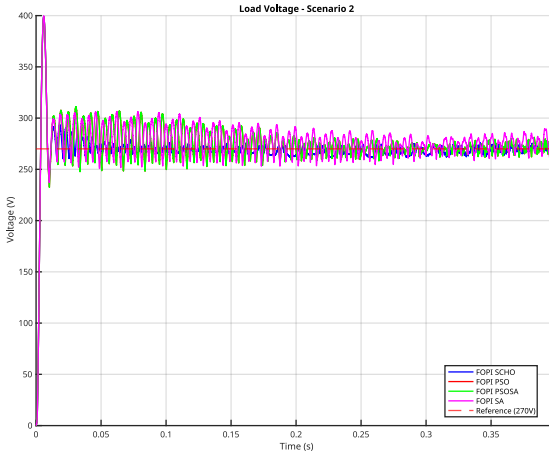

Scenario 1-Group 1: Voltage Measurement

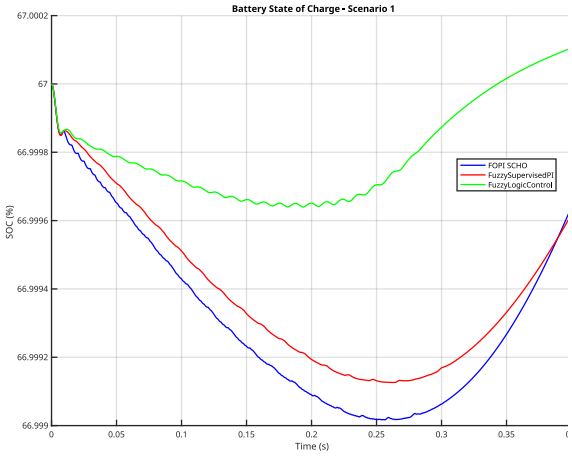

Scenario 1-Group 2: State of Charge Distribution

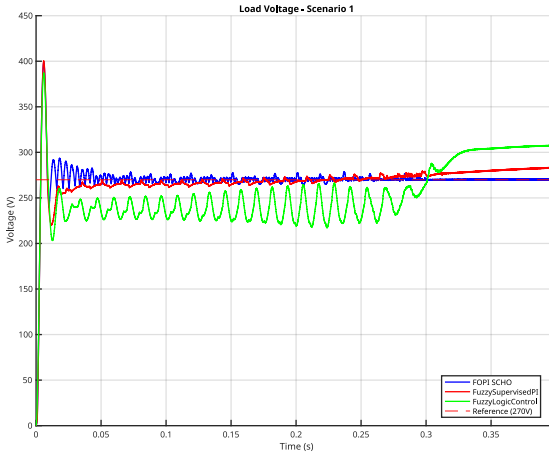

Scenario 1-Group 2: Voltage Measurement

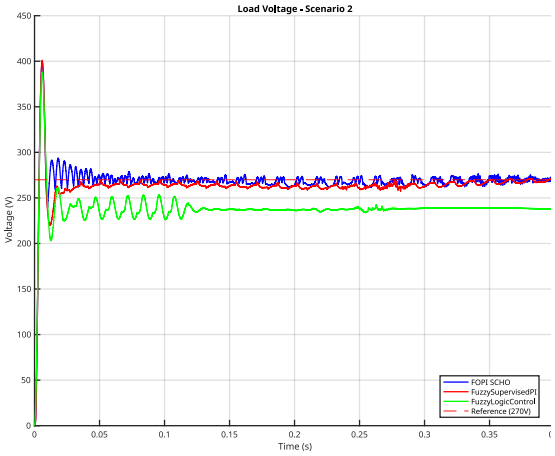

Scenario 2-Group 2: Voltage Measurement

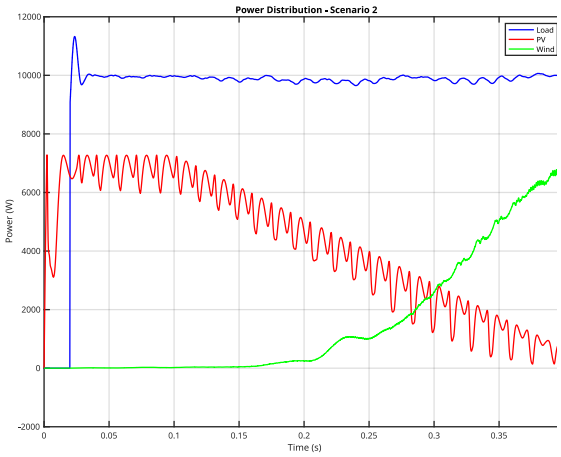

Scenario 2-Group 1: Power Distribution

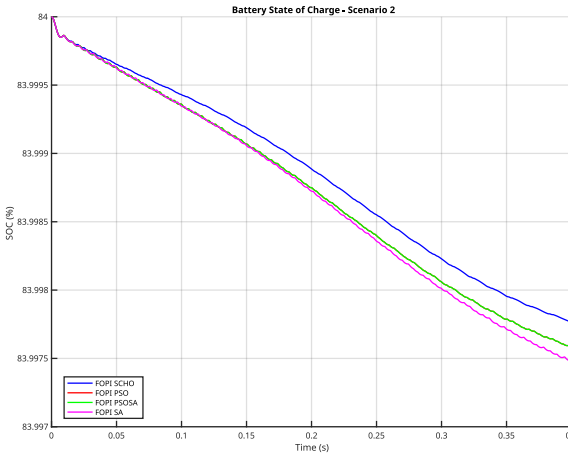

Scenario 2-Group 1: State of Charge Distribution

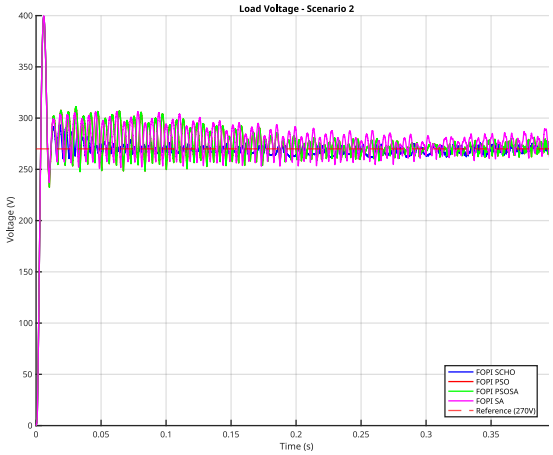

Scenario 2-Group 1: Voltage Measurement

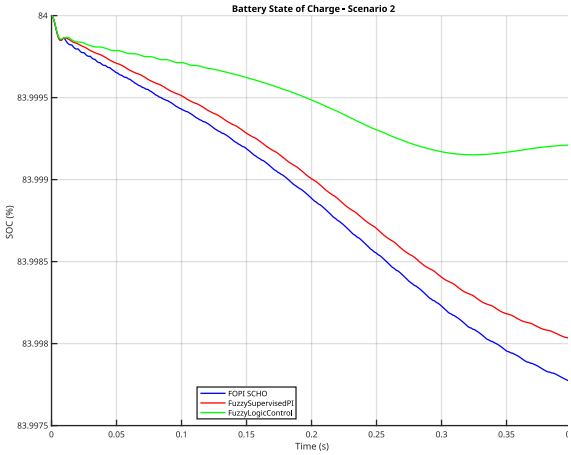

Scenario 2-Group 2: State of Charge Distribution

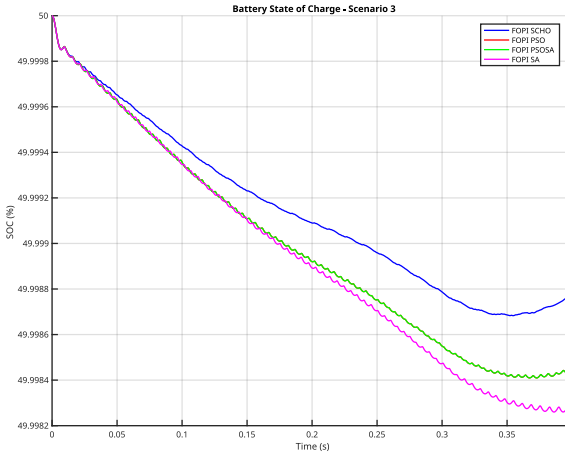

Scenario 3-Group 1: State of Charge Distribution

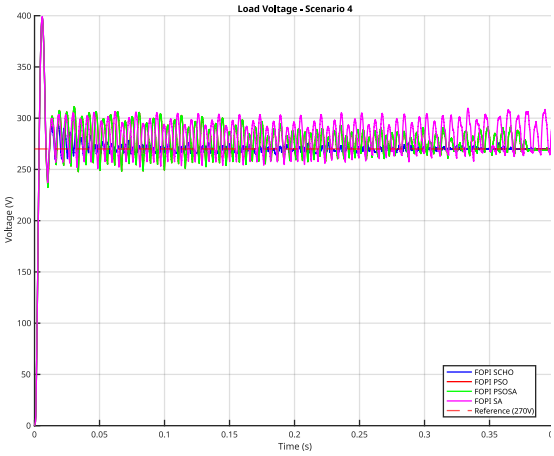

Scenario 3-Group 1: Voltage Measurement

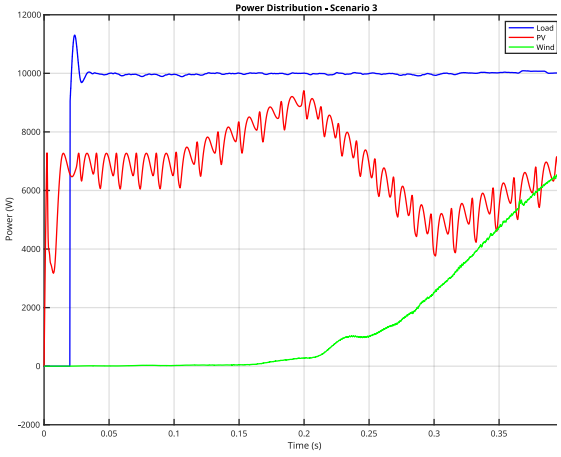

Scenario 3-Group 1: Power Distribution

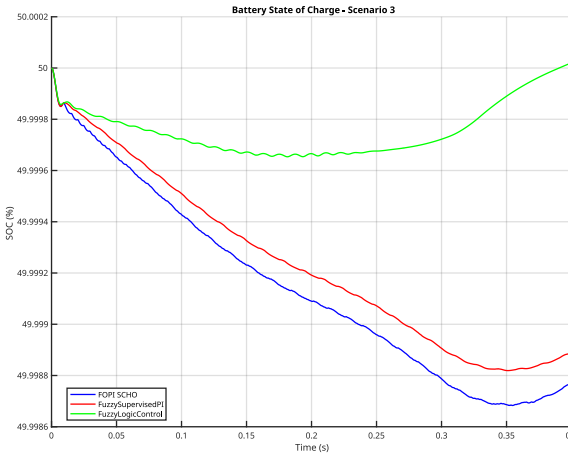

Scenario 3-Group 2: State of Charge Distribution

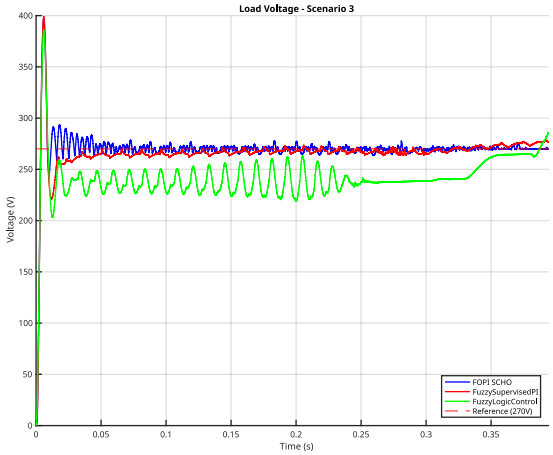

Scenario 3-Group 2: Voltage Measurement

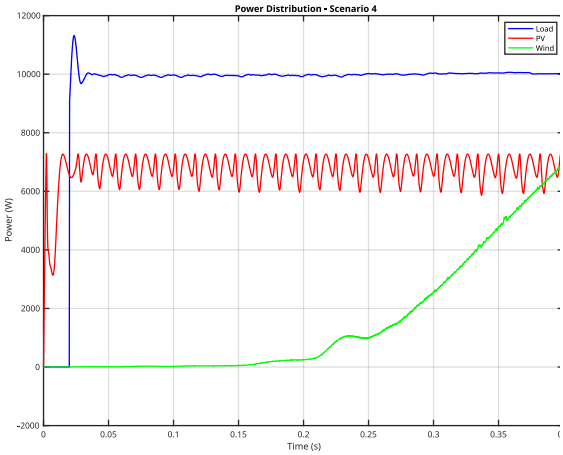

Scenario 4-Group 1: Power Distribution

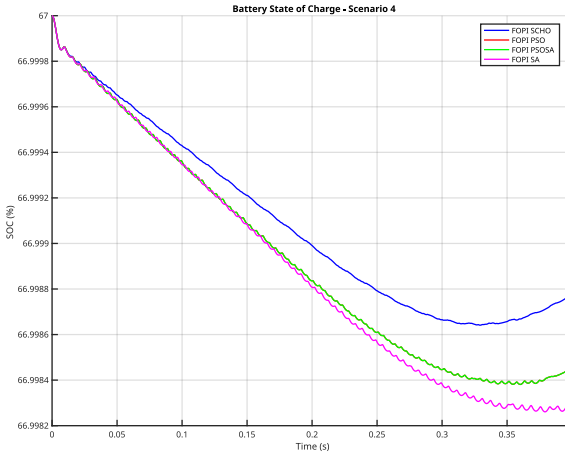

Scenario 4-Group 1: State of Charge Distribution

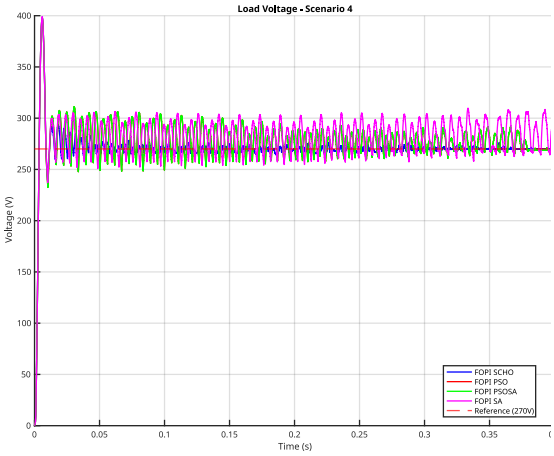

Scenario 4-Group 1: Voltage Measurement

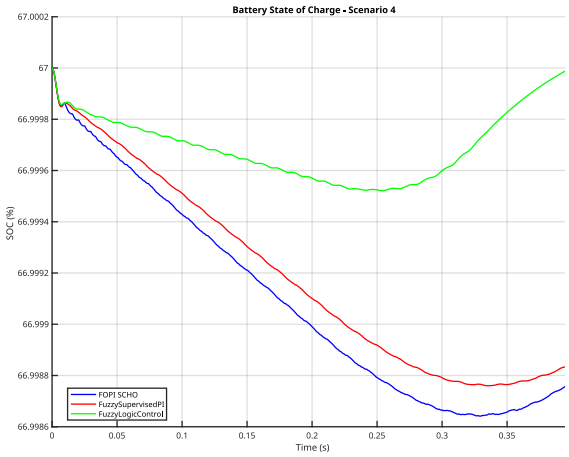

Scenario 4-Group 2: State of Charge Distribution

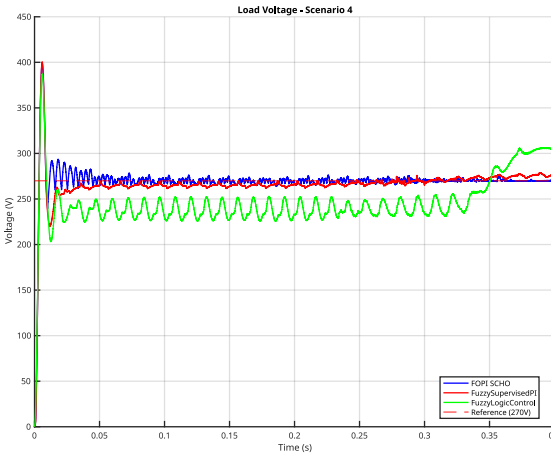

Scenario 4-Group 2: Voltage Measurement

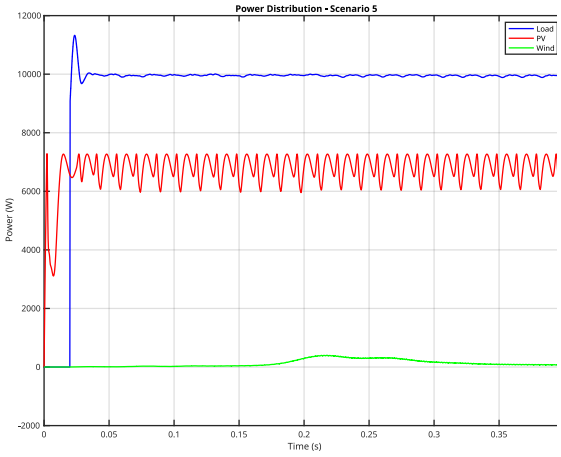

Scenario 5-Group 1: Power Distribution

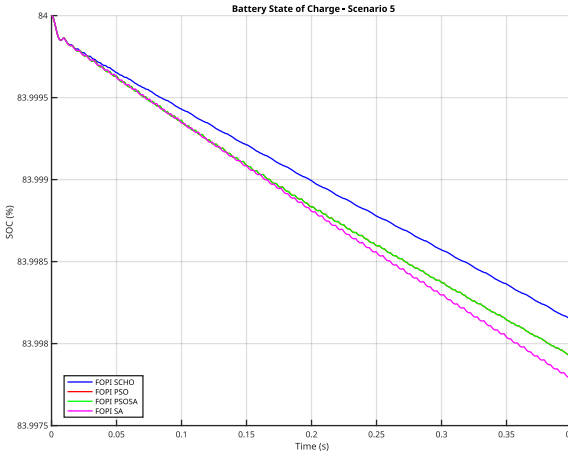

Scenario 5-Group 1: State of Charge Distribution

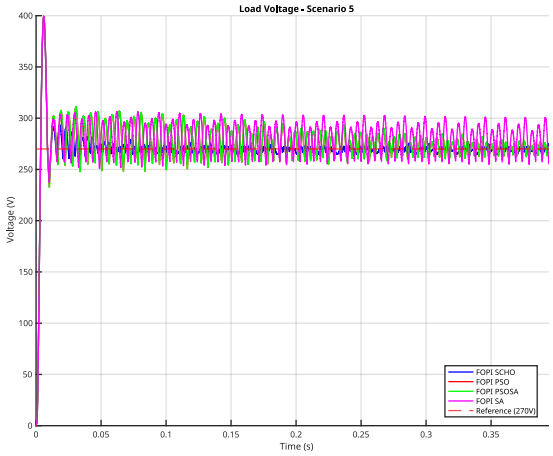

Scenario 5-Group 1: Voltage Measurement

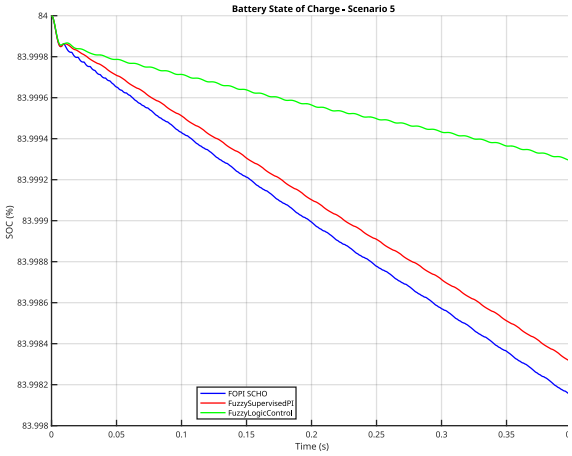

Scenario 5-Group 2: State of Charge Distribution

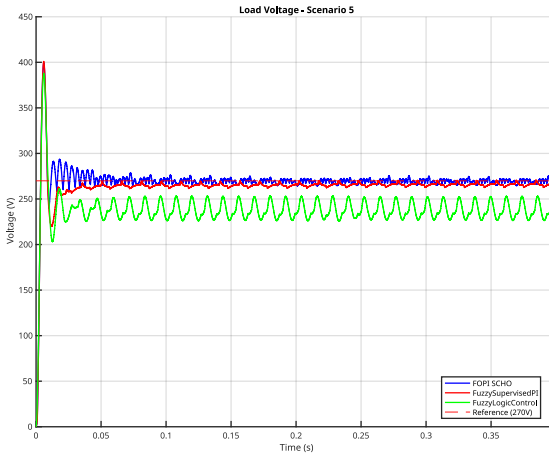

Scenario 5-Group 2: Voltage Measurement

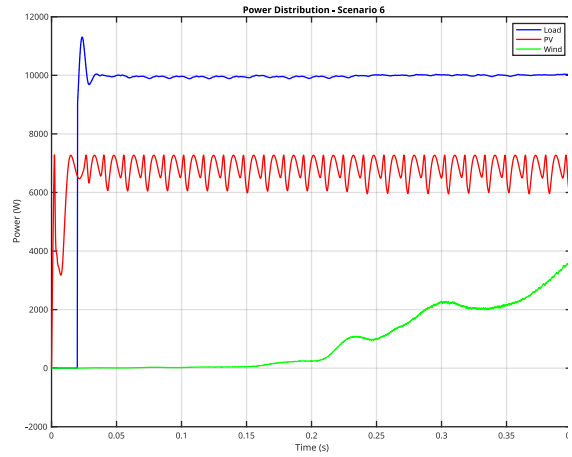

Scenario 6-Group 1: State of Charge Distribution

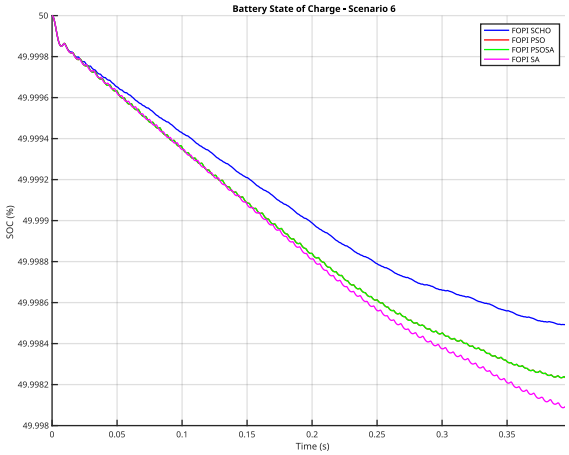

Scenario 6-Group 1: Voltage Measurement

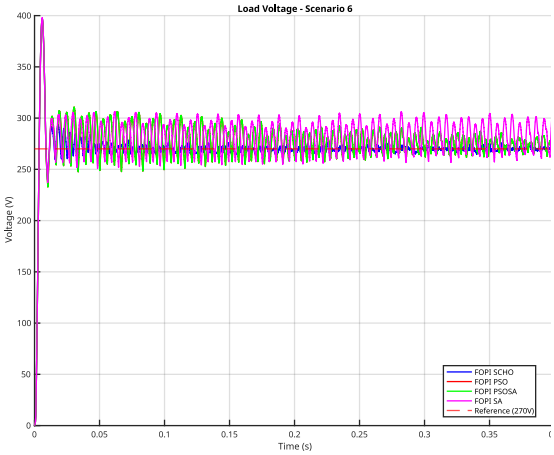

Scenario 6-Group 1: Voltage Measurement

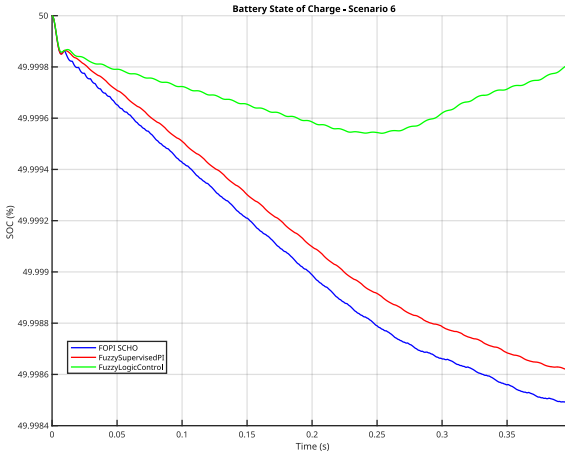

Scenario 6-Group 2: State of Charge Distribut

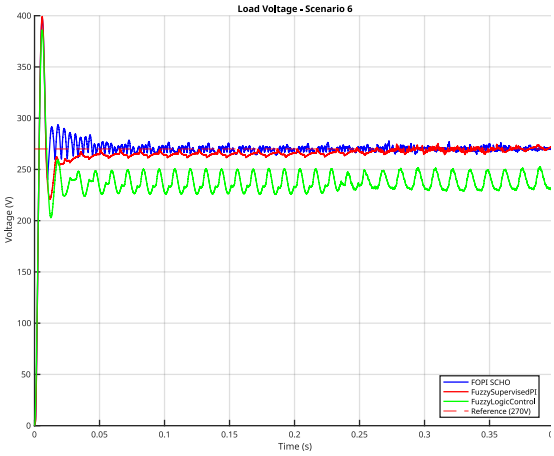

Scenario 6-Group 2: Voltage Measurement

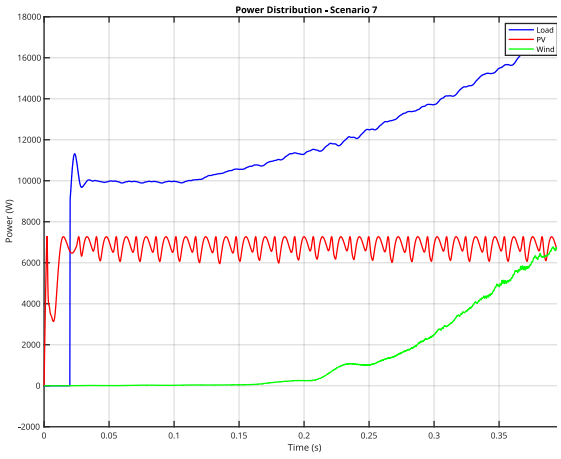

Scenario 7-Group 1: Power Distribution

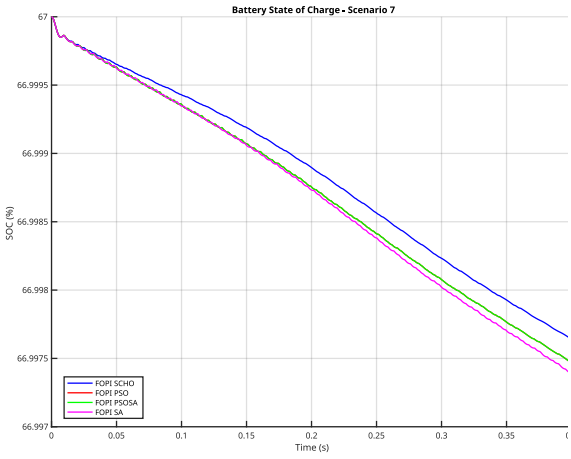

Scenario 7-Group 1: State of Charge Distribution

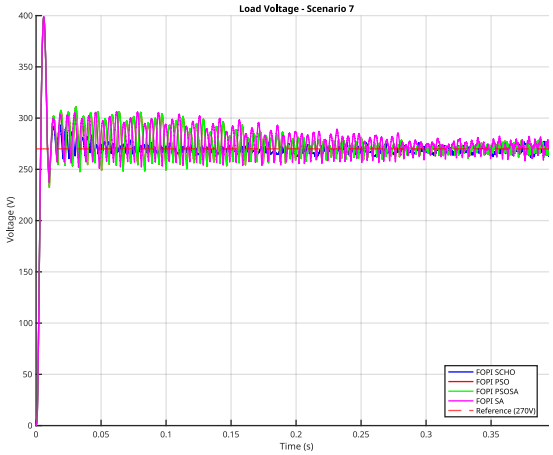

Scenario 7-Group 1: Voltage Measurement

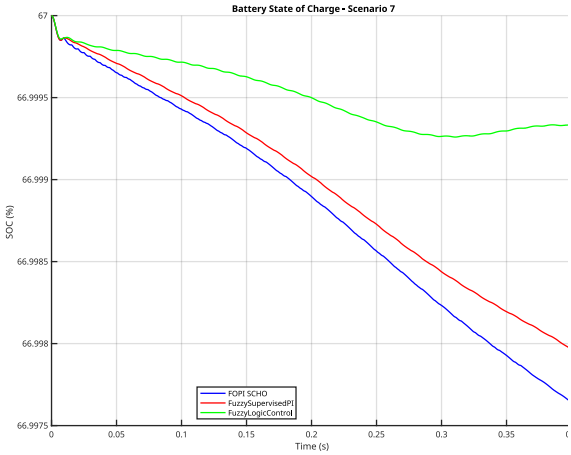

Scenario 7-Group 2: State of Charge Distribution

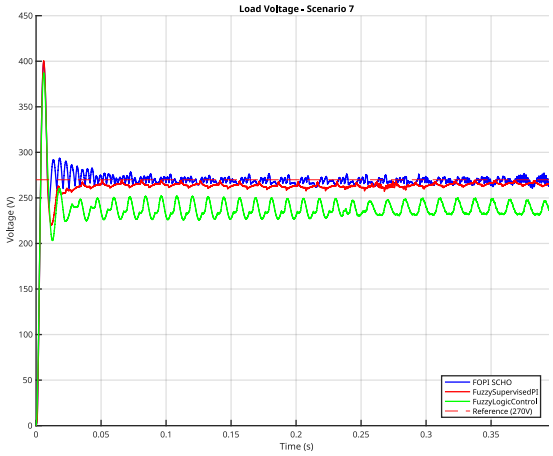

Scenario 7-Group 2: Voltage Measurement

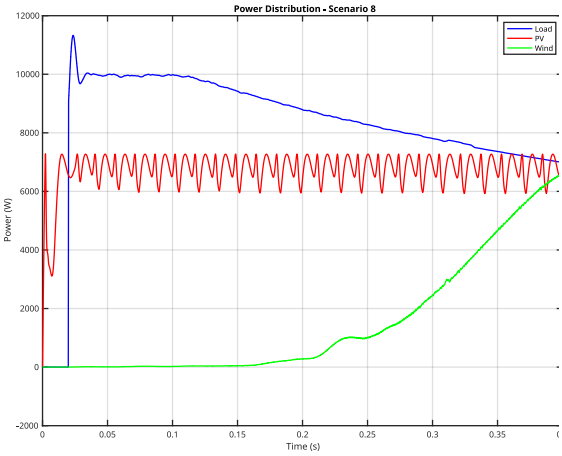

Scenario 8-Group 1: Power Distribution

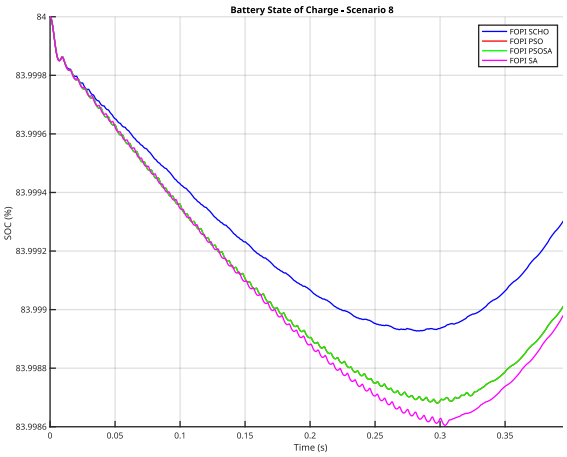

Scenario 8-Group 1: State of Charge Distribution

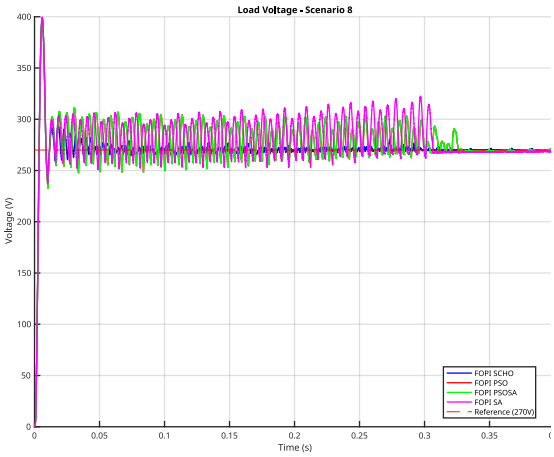

Scenario 8-Group 1: Voltage Measurement

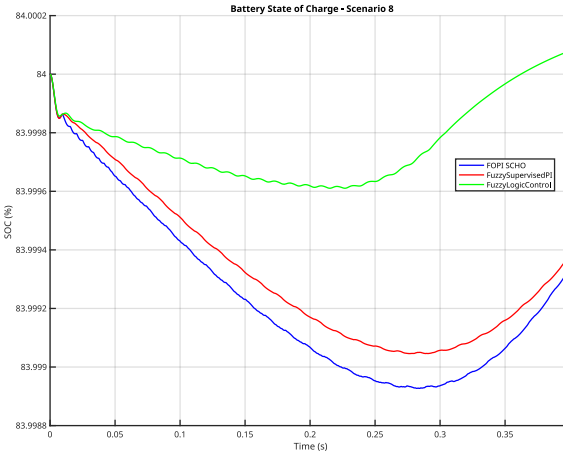

Scenario 8-Group 2: State of Charge Distribution

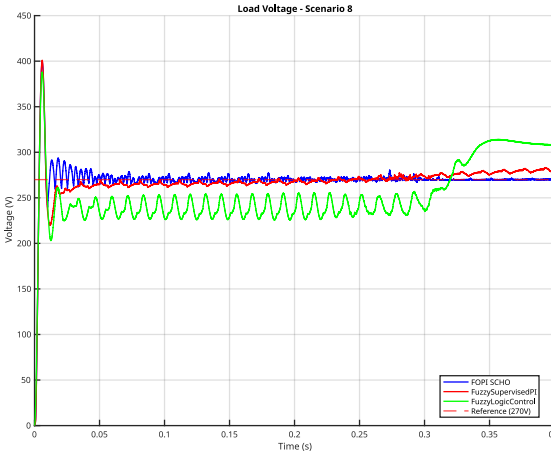

Scenario 8-Group 2: Voltage Measurement

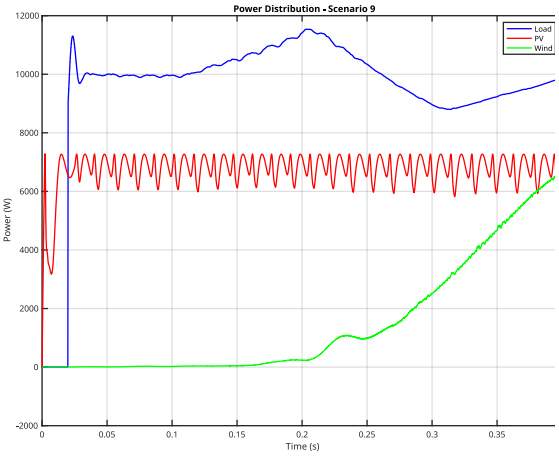

Scenario 9-Group 1: Power Distribution

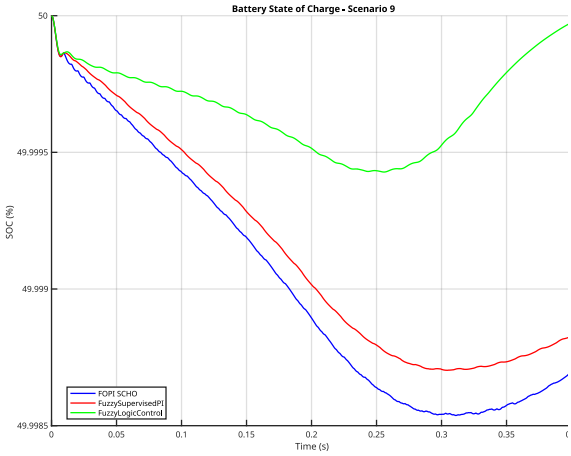

Scenario 9-Group 2: State of Charge Distribution

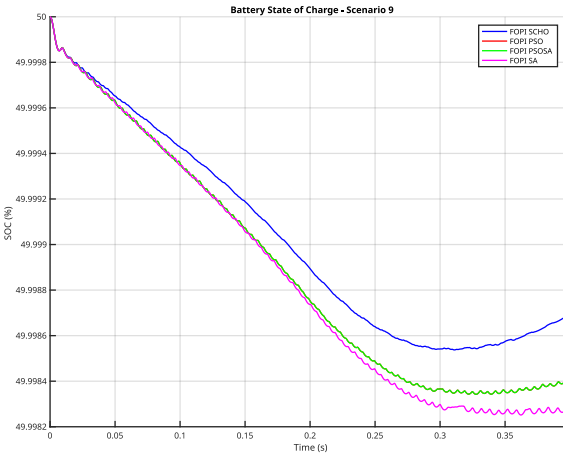

Scenario 9-Group 1: State of Charge Distribution

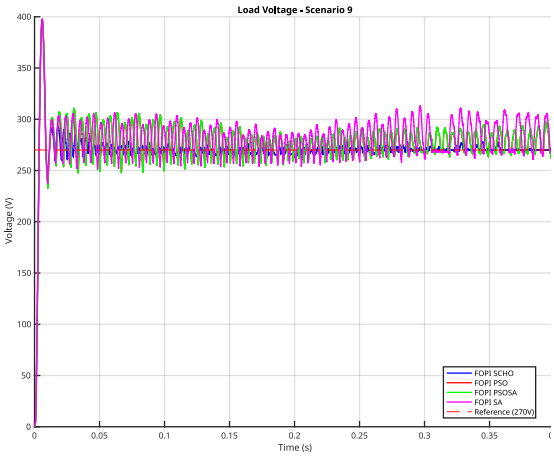

Scenario 9-Group 1: Voltage Measurement

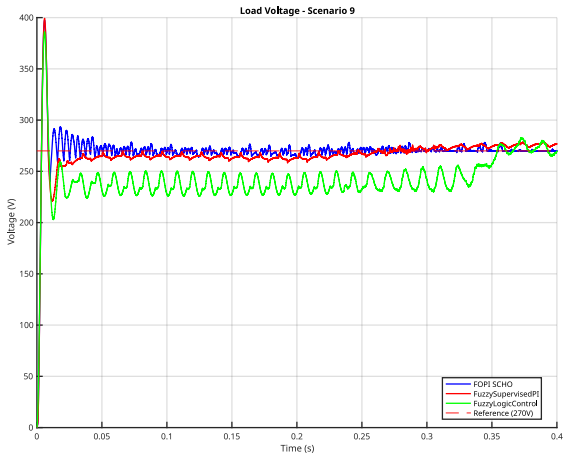

Scenario 9-Group 2: Voltage Measurement

References

[1] M. S. Alam *et al.*, "Renewable energy integration with DC microgrids: Challenges and opportunities," *Electric Power Systems Research,* vol. 234, p. 110548, 2024.

[2] V. F. Pires, A. Pires, and A. Cordeiro, "DC microgrids: benefits, architectures, perspectives and challenges," *Energies,* vol. 16, no. 3, p. 1217, 2023.

[3] R. Maurya, S. Prakash, and A. K. Singh, "Challenges, configuration, control, and scope of DC microgrid systems: a review," *Journal of Electrical Engineering Technology,* vol. 18, no. 3, pp. 1655-1674, 2023.

[4] E. Hernández-Mayoral *et al.*, "A comprehensive review on power-quality issues, optimization techniques, and control strategies of microgrid based on renewable energy sources," *Sustainability,* vol. 15, no. 12, p. 9847, 2023.

[5] K. Kant and O. H. Gupta, "DC microgrid: a comprehensive review on protection challenges and schemes," *IETE Technical Review,* vol. 40, no. 4, pp. 574-590, 2023.

[6] R. Kumar and N. Sinha, "Voltage stability of solar dish-Stirling based autonomous DC microgrid using grey wolf optimised FOPID-controller," *International Journal of Sustainable Energy,* vol. 40, no. 5, pp. 412-429, 2021.

[7] B. S. Goud, C. R. Reddy, M. Bajaj, E. E. Elattar, and S. Kamel, "Power quality improvement using distributed power flow controller with BWO-based FOPID controller," *Sustainability,* vol. 13, no. 20, p. 11194, 2021.

[8] A. M. Nassef, M. A. Abdelkareem, H. M. Maghrabie, and A. Baroutaji, "Metaheuristic-based algorithms for optimizing fractional-order controllers—a recent, systematic, and comprehensive review," *Fractal Fractional,* vol. 7, no. 7, p. 553, 2023.

[9] S. Kaur, Y. Kumar, A. Koul, and S. Kumar Kamboj, "A systematic review on metaheuristic optimization techniques for feature selections in disease diagnosis: open issues and challenges," *Archives of Computational Methods in Engineering,* vol. 30, no. 3, pp. 1863-1895, 2023.

[10] J. Bai *et al.*, "A sinh cosh optimizer," *Knowledge-Based Systems,* vol. 282, p. 111081, 2023.

[11] X. Wang, Y. Wei, Z. Guo, J. Wang, H. Yu, and B. Hu, "A Sinh–Cosh-Enhanced DBO Algorithm Applied to Global Optimization Problems," *Biomimetics,* vol. 9, no. 5, p. 271, 2024.

[12] R. A. Ibrahim, M. A. S. Aly, Y. S. Moemen, I. E. T. El Sayed, M. Abd Elaziz, and H. A. J. C. Khalil, "Boosting Sinh Cosh Optimizer and arithmetic optimization algorithm for improved prediction of biological activities for indoloquinoline derivatives," *Chemosphere,* vol. 359, p. 142362, 2024.

[13] M. Esmaeili, A. A. Ahmadi, A. Nateghi, and M. Shafie-khah, "Robust power management system with generation and demand prediction and critical loads in DC microgrid," *Journal of Cleaner Production,* vol. 384, p. 135490, 2023.

[14] B. A. Fadheel *et al.*, "A Hybrid Sparrow Search Optimized Fractional Virtual Inertia Control for Frequency Regulation of Multi-Microgrid System," *IEEE Access,* 2024.

[15] F. Gul, I. Mir, W. Rahiman, and T. U. Islam, "Novel implementation of multi-robot space exploration utilizing coordinated multi-robot exploration and frequency modified whale optimization algorithm," *IEEE Access,* vol. 9, pp. 22774-22787, 2021.
[16] J. Xu and L. Xu, "Optimal stochastic process optimizer: A new metaheuristic algorithm with adaptive exploration-exploitation property," *IEEE Access,* vol. 9, pp. 108640-108664, 2021.
[17] D. Zhang, Z. Wang, Y. Zhao, and F. Sun, "Multi-Strategy Fusion Improved Dung Beetle Optimization Algorithm and Engineering Design Application," *IEEE Access,* 2024.
[18] A. Prasanthi, H. Shareef, R. Errouissi, M. Asna, and A. Wahyudie, "Quantum chaotic butterfly optimization algorithm with ranking strategy for constrained optimization problems," *IEEE Access,* vol. 9, pp. 114587-114608, 2021.
[19] H. T. Sadeeq and A. M. Abdulazeez, "Giant trevally optimizer (GTO): A novel metaheuristic algorithm for global optimization and challenging engineering problems," *Ieee Access,* vol. 10, pp. 121615-121640, 2022.
[20] H. Givi, M. Dehghani, and Š. J. I. A. Hubálovský, "Red panda optimization algorithm: An effective bio-inspired metaheuristic algorithm for solving engineering optimization problems," *IEEE Access,* vol. 11, pp. 57203-57227, 2023.
[21] T. Dutta, S. Bhattacharyya, S. Dey, and J. Platos, "Border collie optimization," *IEEE access,* vol. 8, pp. 109177-109197, 2020.
[22] A. Fatani, M. Abd Elaziz, A. Dahou, M. A. Al-Qaness, and S. Lu, "IoT intrusion detection system using deep learning and enhanced transient search optimization," *IEEE Access,* vol. 9, pp. 123448-123464, 2021.
[23] A. Tang, H. Zhou, T. Han, and L. Xie, "A modified manta ray foraging optimization for global optimization problems," *IEEE Access,* vol. 9, pp. 128702-128721, 2021.
[24] B. Krishna and V. Karthikeyan, "Ultra-voltage gain step-up DC-DC converter for renewable energy micro-source applications," *IEEE Transactions on Energy Conversion,* vol. 37, no. 2, pp. 947-957, 2021.
[25] H. Cui, X. Dong, H. Deng, M. Dehghani, K. Alsubhi, and H. M. A. Aljahdali, "Cyber attack detection process in sensor of DC micro-grids under electric vehicle based on Hilbert–Huang transform and deep learning," *IEEE Sensors Journal,* vol. 21, no. 14, pp. 15885-15894, 2020.
[26] Y. Guan, C. Cecati, J. M. Alonso, and Z. Zhang, "Review of high-frequency high-voltage-conversion-ratio DC–DC converters," *IEEE Journal of Emerging Selected Topics in Industrial Electronics,* vol. 2, no. 4, pp. 374-389, 2021.
[27] A. R. Paul, A. Bhattacharya, and K. Chatterjee, "A single-phase grid-connected boost/buck–boost-derived solar PV micro-inverter topology having power decoupling capability," *IEEE Journal of Emerging Selected Topics in Power Electronics,* vol. 11, no. 2, pp. 2340-2349, 2023.
[28] Z. Elgamal, A. Q. M. Sabri, M. Tubishat, D. Tbaishat, S. N. Makhadmeh, and O. A. Alomari, "Improved reptile search optimization algorithm using chaotic map and simulated annealing for feature selection in medical field," *IEEE Access,* vol. 10, pp. 51428-51446, 2022.
[29] K. Kanathipan and J. Lam, "A high voltage gain isolated PV micro-converter with a single-voltage maximum power point tracking control loop for DC micro-grid systems," *IEEE Journal of Emerging Selected Topics in Industrial Electronics,* vol. 3, no. 3, pp. 755-765, 2021.
[30] Y. Liang, H. Zhang, M. Du, and K. Sun, "Parallel coordination control of multi-port DC-DC converter for stand-alone photovoltaic-energy storage systems," *CPSS Transactions on Power Electronics Applications,* vol. 5, no. 3, pp. 235-241, 2020.
[31] W. Lambrichts and M. Paolone, "Linear recursive state estimation of hybrid and unbalanced ac/dc micro-grids using synchronized measurements," *IEEE Transactions on Smart Grid,* vol. 14, no. 1, pp. 54-67, 2022.
[32] Y. Khayat, S. Golestan, J. M. Guerrero, J. C. Vasquez, and H. Bevrani, "DC-link voltage control aided for the inertial support during severe faults in weak grids," *IEEE Journal of Emerging Selected Topics in Power Electronics,* vol. 9, no. 6, pp. 7296-7305, 2020.
[33] F. M. Shah, S. Maqsood, Z. M. Shah, F. Muhammad, and S. Kim, "Multilevel LVDC distribution system with voltage unbalancing and disturbance rejection control topology," *IEEE Access,* vol. 8, pp. 133787-133801, 2020.

[34] Z. Xia, M. Su, Z. Liu, R. Liu, and Y. Liu, "Existence conditions and stability for the power-flow of DC micro-grids with CPLs," *IEEE Transactions on Smart Grid,* vol. 13, no. 6, pp. 4284-4299, 2022.

[35] J. A. Rohten *et al.*, "A simple self-tuning resonant control approach for power converters connected to micro-grids with distorted voltage conditions," *IEEE Access,* vol. 8, pp. 216018-216028, 2020.

[36] Z. Karami, Q. Shafiee, S. Sahoo, M. Yaribeygi, H. Bevrani, and T. Dragicevic, "Hybrid model predictive control of DC–DC boost converters with constant power load," *IEEE Transactions on Energy Conversion,* vol. 36, no. 2, pp. 1347-1356, 2020.

[37] A. Rajamallaiah, S. P. K. Karri, and Y. R. Sankar, "Deep Reinforcement Learning Based Control Strategy for Voltage Regulation of DC-DC Buck Converter Feeding CPLs in DC Microgrid," *IEEE Access,* 2024.

[38] V. Kumar, D. Kumar, M. Kaur, D. Singh, S. A. Idris, and H. Alshazly, "A novel binary seagull optimizer and its application to feature selection problem," *IEEE Access,* vol. 9, pp. 103481-103496, 2021.

[39] M. Naderi, Y. Khayat, Q. Shafiee, T. Dragičević, H. Bevrani, and F. Blaabjerg, "Interconnected autonomous ac microgrids via back-to-back converters—Part II: Stability analysis," *IEEE Transactions on Power Electronics,* vol. 35, no. 11, pp. 11801-11812, 2020.

[40] B. K. Gupta, K. R. Sekhar, and A. I. Gedam, "Solar interfaced series inverter with provision of common DC bus grounding," *IEEE Transactions on Industrial Electronics,* vol. 69, no. 4, pp. 3656-3666, 2021.

[41] Y.-H. Jia, Y. Mei, and M. Zhang, "A two-stage swarm optimizer with local search for water distribution network optimization," *IEEE Transactions on Cybernetics,* vol. 53, no. 3, pp. 1667-1681, 2021.

[42] Y. Zheng, Y. Wang, X. Meng, S. Li, and H. Chen, "Distributed Economic MPC for Synergetic Regulation of the Voltage of an Island DC Micro-Grid," *IEEE/CAA Journal of Automatica Sinica,* vol. 11, no. 3, pp. 734-745, 2024.

[43] A. S. Desuky, S. Hussain, S. Kausar, M. A. Islam, and L. M. El Bakrawy, "EAOA: an enhanced archimedes optimization algorithm for feature selection in classification," *IEEE Access,* vol. 9, pp. 120795-120814, 2021.

[44] Z. Karami, Q. Shafiee, Y. Khayat, M. Yaribeygi, T. Dragičević, and H. Bevrani, "Decentralized model predictive control of DC microgrids with constant power load," *IEEE Journal of Emerging Selected Topics in Power Electronics,* vol. 9, no. 1, pp. 451-460, 2019.

[45] L. Sun, W. Jiang, S. Hashimoto, Z. Lin, and T. Kawaguchi, "Multi-port Energy Router for DC Grid Clusters," *IEEE Journal of Emerging Selected Topics in Power Electronics,* 2024.

[46] P. Danner, A. Volkova, and H. De Meer, "Two-Step Blackout Mitigation by Flexibility-Enabled Microgrid Islanding," in *Proceedings of the 15th ACM International Conference on Future and Sustainable Energy Systems*, 2024, pp. 596-605.

[47] K. Suresh and E. Parimalasundar, "IPWM based IBMSC DC-AC converter using solar power for wide voltage conversion system convertisseur DC-AC IBMSC basé sur l'IPWM et utilisant l'énergie solaire pour un système de conversion à large tension," *IEEE Canadian Journal of Electrical Computer Engineering,* vol. 45, no. 4, pp. 394-400, 2022.

[48] V. Chapparya, A. Dey, and S. P. Singh, "A novel non-isolated boost-zeta interleaved DC-DC converter for low voltage bipolar DC micro-grid application," *IEEE Transactions on Industry Applications,* vol. 59, no. 5, pp. 6182-6192, 2023.

[49] S. Li, Y. Jiang, B. Fang, and C. Wang, "Characteristics analysis of inertia damping of grid-connected system of direct-drive wind power generation," *IEEE Access,* vol. 8, pp. 189802-189810, 2020.

[50] N. R. Merritt, C. Chakraborty, P. Bajpai, and B. C. Pal, "A unified control structure for grid connected and islanded mode of operation of voltage source converter based distributed generation units under unbalanced and non-linear conditions," *IEEE Transactions on Power Delivery,* vol. 35, no. 4, pp. 1758-1768, 2019.

[51] X. Chen, R. Tian, Y. Wang, S. Xu, W. Jiang, and S. Hashimoto, "A Novel Voltage-Current Dual-Drop Control Method for Shipboard DC Micro-Grid with Energy Storage Systems," *IEEE Access,* 2024.

[52] K. Hussain, W. Zhu, and M. N. M. Salleh, "Long-term memory Harris' hawk optimization for high dimensional and optimal power flow problems," *IEEE access,* vol. 7, pp. 147596-147616, 2019.

[53] A. Tiwari, "A hybrid feature selection method using an improved binary butterfly optimization algorithm and adaptive β–hill climbing," *IEEE Access,* vol. 11, pp. 93511-93537, 2023.

[54] Y.-H. Chou, S.-Y. Kuo, L.-S. Yang, and C.-Y. Yang, "Next generation metaheuristic: Jaguar algorithm," *IEEE Access,* vol. 6, pp. 9975-9990, 2018.

[55] M. Qaraad, S. Amjad, N. K. Hussein, S. Mirjalili, N. B. Halima, and M. A. Elhosseini, "Comparing SSALEO as a scalable large scale global optimization algorithm to high-performance algorithms for real-world constrained optimization benchmark," *IEEE Access,* vol. 10, pp. 95658-95700, 2022.